



Memory consolidation and improvement by synaptic tagging and capture in recurrent neural networks

Jannik Luboeinski ^{1,2}✉ & Christian Tetzlaff ^{1,2}✉

The synaptic-tagging-and-capture (STC) hypothesis formulates that at each synapse the concurrence of a tag with protein synthesis yields the maintenance of changes induced by synaptic plasticity. This hypothesis provides a biological principle underlying the synaptic consolidation of memories that is not verified for recurrent neural circuits. We developed a theoretical model integrating the mechanisms underlying the STC hypothesis with calcium-based synaptic plasticity in a recurrent spiking neural network. In the model, calcium-based synaptic plasticity yields the formation of strongly interconnected cell assemblies encoding memories, followed by consolidation through the STC mechanisms. Furthermore, we show for the first time that STC mechanisms modify the storage of memories such that after several hours memory recall is significantly improved. We identify two contributing processes: a merely time-dependent passive improvement, and an active improvement during recall. The described characteristics can provide a new principle for storing information in biological and artificial neural circuits.

¹Department of Computational Neuroscience, III. Institute of Physics-Biophysics, University of Göttingen, Göttingen, Germany. ²Bernstein Center for Computational Neuroscience, Göttingen, Germany. ✉email: jannik.luboeinski@phys.uni-goettingen.de; tetzlaff@phys.uni-goettingen.de

In biological neural systems, memories have a wide repertoire of dynamics; most importantly, they can be encoded, stored, recalled, and consolidated. While these dynamics are relatively well-explored at the behavioral and brain-region level^{1–3}, the underlying synaptic and neuronal processes remain mainly elusive.

Most generally, learning describes the ability of humans and other animals to obtain knowledge about an entity. This knowledge or information is stored as a memory. The encoding of such a memory in a neural network is commonly assumed to happen in the way as described by Hebb in his seminal work^{4–6}: a group of recurrently connected neurons that receives the information by an external input starts to fire stronger than the rest of the network. This increased firing yields strengthening of the efficacy of the recurrent synapses within this particular group such that a so-called Hebbian cell assembly is formed, which represents a memory of the input. On the other hand, low firing rates typically cause weakening of connections between neurons, which can lead to either disruption or refinement of a cell assembly. Strengthening and weakening of synapses at timescales relevant to memory is the result of long-term synaptic plasticity^{7–9}.

Long-term synaptic plasticity creates long-lasting changes of the synaptic efficacy. To become strengthened, synapses undergo a cascade of molecular processes that leads to an increase in the number of postsynaptic receptors, which is called long-term potentiation (LTP, refs. 9–12). Analogously, for weakening, another cascade of processes yields a decrease in the number of receptors, which is called long-term depression (LTD, refs. 9,10,12). The signaling cascades of both LTP and LTD are triggered by the calcium concentration in the postsynaptic spine. The spiking activities of the presynaptic and the postsynaptic neurons drive the calcium concentration and, by this, determine whether LTP or LTD of the synaptic efficacy is induced^{7,13–16}. In general, long-term synaptic plasticity consists of at least two different phases. Changes of the synaptic efficacy in the early phase last for several hours, while efficacy changes in the late phase can be maintained for several days^{11,17}. The transfer from the early to the late phase has been described by the synaptic-tagging-and-capture (STC) hypothesis^{18,19}. Following the STC hypothesis, the transfer depends on the stimulation of the specific synapse, as well as on the stimulation of other synapses at the same postsynaptic neuron. More precisely, the transfer at a synapse occurs if the synapse is tagged, which means that it is primed for transfer, and if proteins necessary for the late phase are abundant or have been synthesized. The tagged synapse then “captures” proteins causing the transfer to the late phase by increasing for instance the number of receptor slots at the postsynaptic site¹⁹. The formation of a tag at a synapse is related to its own early-phase change, while protein synthesis depends on the early-phase state of many synapses^{15,18–20}. The total or effective synaptic efficacy of a synapse consists of the sum of the early- and late-phase contribution^{15,20}.

In general, consolidation of memories means the progressive transfer of memories into a state in which they stay stable over long time intervals^{1,3,21}. There are two major categories of memory consolidation: systems consolidation and synaptic (or initial) consolidation^{1,22}. The basic idea of systems consolidation is that a memory is transiently stored in the hippocampus and possibly transferred to the neocortex, in which it is maintained for a longer period. The question, whether a memory is first encoded in the hippocampus and then transferred to the neocortex or whether the encoding of a memory occurs simultaneously in both regions (multiple trace theory, refs. 1,23), is subject to an ongoing debate. In both cases, however, the newly formed memory has to be initially consolidated before systems consolidation sets in. This initial consolidation process is related to local molecular and

cellular processes at individual neurons and synapses, and is therefore named synaptic consolidation^{24–26}.

The STC hypothesis provides a potential explanation of the neuronal and synaptic processes underlying the synaptic consolidation of memories^{1,18,19}, which is supported by several theoretical studies focusing on single synapses or feed-forward networks^{12,15,20,27,28}. However, a clear link between the STC hypothesis and memory consolidation is still missing as the encoding of memories in neural circuits is mainly associated with strongly recurrently connected groups of neurons (cell assemblies). Another study of recurrent networks with multiple cell assemblies already found that cue-triggered recall was only possible after 20 min if a type of synaptic consolidation was present²⁹.

In this study, we developed a theoretical model of recurrently connected spiking neurons with the synaptic efficacies being altered by calcium-dependent synaptic plasticity and the core mechanisms of the STC hypothesis. The individual components of the implemented model reproduce various plasticity phenomena as the ones described above^{18,30–39}, and for verification, we matched the temporal evolution of individual synapses in our model with experimental data. Our network simulations show the synaptic and neuronal dynamics underlying the formation of a memory representation, its recall, and its long-term development. The latter indicates that the STC mechanisms in a recurrent circuit lead to the consolidation of a memory. Finally, the simulations and analytical results suggest a new implication of the STC mechanisms on memory representations, which is the enhancement of the storage of the memory. This enhancement exhibits a new type of memory dynamics, which could be beneficial for biological, as well as for artificial memory systems.

Previous theoretical studies^{40–43} investigated general computational principles emerging from multiple-timescale plasticity. For instance, using rather abstract models of multiple-timescale plasticity based on binary⁴⁰ and discrete-valued⁴² synaptic weights, Elliott and colleagues predicted the possibility of the improvement in memory strength with the passage of time. However, the underlying dynamics have not been linked to specific biological mechanisms. While Papper et al.⁴⁴ identified that STC mechanisms can trigger an improvement in memory lifetime, we show that improvement in memory strength can also be related to the biologically plausible mechanisms of STC together with calcium-dependent plasticity.

Results

We aimed to set up a biophysically plausible network model of the neuronal and synaptic dynamics underlying synaptic consolidation. For this, based on previous studies^{13,15,20}, we utilized a synaptic model that integrates the local calcium dynamics to trigger synaptic plasticity, and the mechanisms of STC (Fig. 1a). We used this synaptic model in conjunction with a leaky integrate-and-fire model, axonal delay, and a finite synaptic time constant to cover the most important aspects of signal generation and transmission in neural networks, with parameters based on experimental findings (see “Methods” section, refs. 45,46). The network itself was sparsely coupled and received input such that it resembled connectivity and firing rates as present in the hippocampus during exploratory wake state (refs. 47–50; see also Supplementary Fig. S3). By applying an additional, strong input stimulus to a particular subset of excitatory neurons, cell assemblies were formed (Fig. 1b). In the following, we will first introduce the key principles of the synapse model and compare its dynamics to experimental data, before we present the characteristics of the network model.

Comparison of synapse model with experimental data. In general, the model assumes that the membrane potential of a

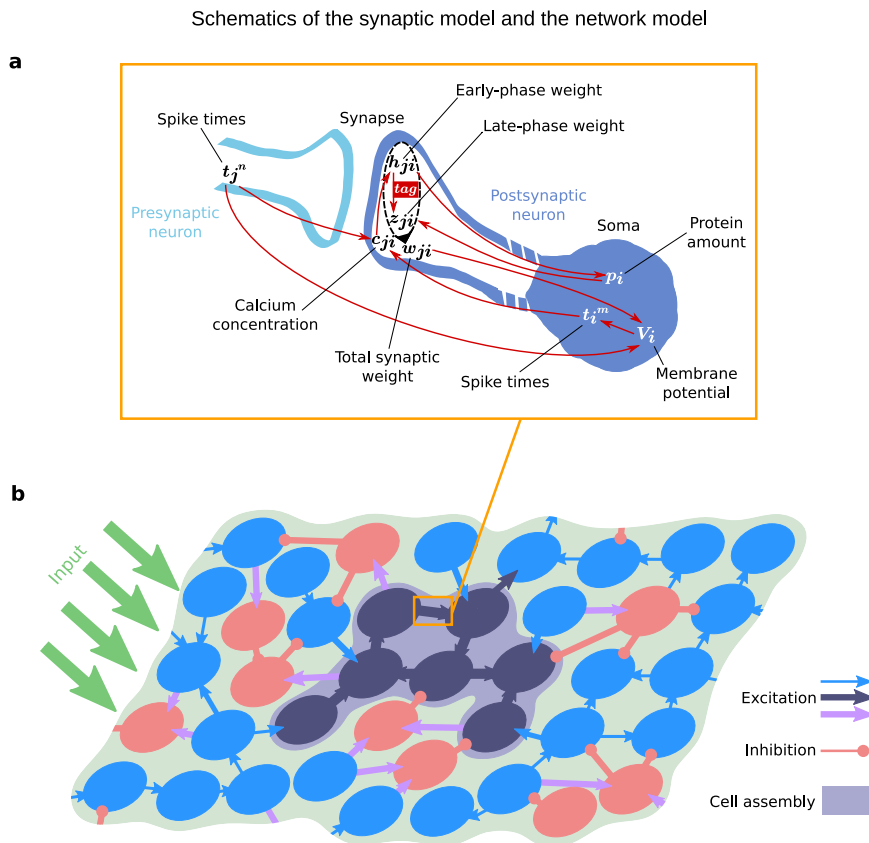


Fig. 1 Schematics of the synaptic model and the network model. **a** The synaptic model integrates the interplay between various mechanisms of calcium-dependent synaptic plasticity and the STC hypothesis. For more details see the main text. **b** Schematic of a part of the neural network that consists of excitatory (blue and dark blue circles) and inhibitory neurons (red circles), and receives external input from other brain areas (green arrows). Only synapses between excitatory neurons (blue and dark blue arrows) undergo plastic changes by the processes shown in **a**. A Hebbian cell assembly represents a memory and consists of a group of strongly interconnected neurons (dark blue).

neuron determines its spiking dynamics, which drives together with presynaptic spiking the postsynaptic calcium concentration (Fig. 1a). The calcium concentration determines the occurrence of early-phase LTP and early-phase LTD, represented by changes in the early-phase component (or weight) of the synaptic efficacy. Large changes of the early-phase weight trigger the formation of a synapse-specific tag. A sufficient body of early-phase changes at many synapses of the postsynaptic neuron triggers protein synthesis. Once an adequate amount of proteins is available and the synapse is tagged, the late-phase component of the synaptic efficacy is altered; thus, the synapse “captures” proteins. The sum of the early- and late-phase weight yields the total synaptic efficacy that determines the magnitude of postsynaptic potentials arriving at the neuron, influencing its membrane potential. The interplay between these different processes is investigated in standard plasticity induction experiments^{19,35,51,52}. In these experiments, a strong tetanus stimulation (STET) is used to induce late-phase potentiation, while weak tetanus stimulation (WTET) is used to induce early-phase potentiation only. For late-phase depression, a strong low-frequency stimulus (SLFS) is used, while for early-phase depression, a weak low-frequency stimulus (WLFS) suffices. As proof of concept of our synaptic model, we reproduced the outcome of these experiments by considering a single plastic synapse between two neurons, and applying similar stimulation protocols to the presynaptic neuron (see Supplementary Fig. S1 for details). The resulting time traces of the synaptic efficacy in response to the four induction protocols (Fig. 2) match the findings from experiments, as discussed above and from previous theoretical studies^{15,20,27,28}. The fluctuations

and local maxima in our STET and SLFS simulations are within the common range for late-phase plasticity paradigms (cf. refs. ^{35,51,52}). The results indicate that our synaptic model provides a reasonable description of the underlying biomolecular dynamics. Thus, based on this synaptic model, in the next step, we will introduce our analysis of the synaptic and neuronal dynamics in a recurrent neural network.

Network model with synaptic consolidation enables functional memory representations. Employing our synaptic model, we simulated a patch of tissue with hippocampal network characteristics, consisting of 2000 neurons with 20% being inhibitory and a 0.1 average probability of two neurons being connected by a synapse (Fig. 1b). Synapses between excitatory neurons (blue, dark blue) feature plasticity mechanisms, as described above. Inhibitory neurons provide feedback inhibition; their connections are nonplastic (purple, red). All neurons in the patch received additional inputs from outside the network, which have particular characteristics for the encoding and recalling of a memory. During learning, a specific stimulus is provided to a group of neurons and should trigger the formation of particularly strong connections between these neurons, which then represent a Hebbian cell assembly or memory (Fig. 1b, dark blue). During recall, only a subset of the group of neurons that received the learning stimulus received specific external stimulation.

To investigate the synaptic and neuronal dynamics implied by the STC mechanisms, throughout this study, we focused on two time spans. We evaluated the state of the neural network ~10 s

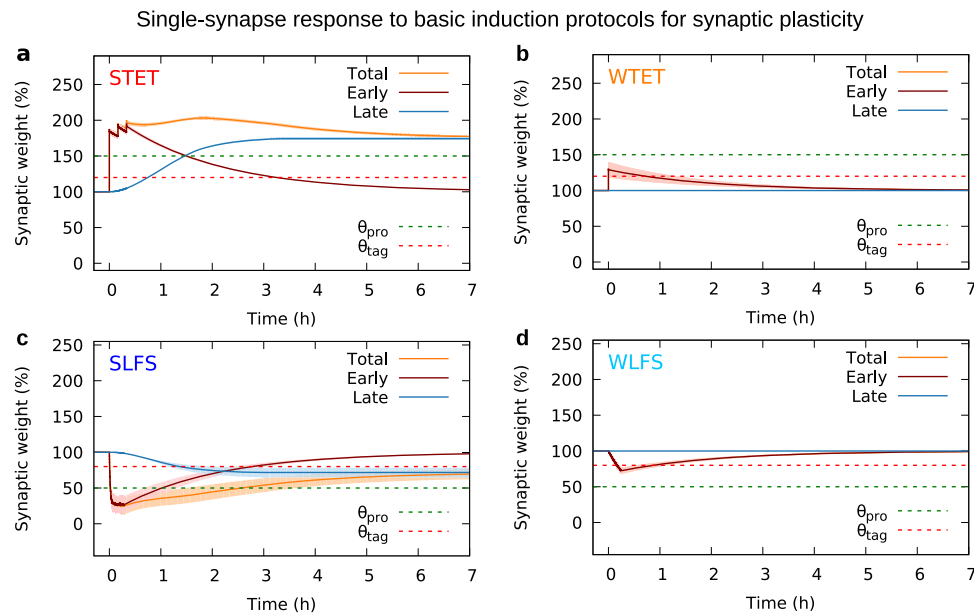


Fig. 2 Impact of strong and weak tetanic and low-frequency stimulation protocols at a single synapse. Each protocol (see Supplementary Fig. S1 for details) leads to the induction of a different type of synaptic plasticity: **a** late-phase potentiation, **b** early-phase potentiation, **c** late-phase depression, and **d** early-phase depression. The late-phase weight (blue line) is only changed by strong stimulation (STET, SLFS). The early-phase weight (red line) is affected by all protocols. Weak stimulation protocols (WTET, WLFS) suffice to drive the early-phase weight across the threshold of tag formation (θ_{tag} , dashed red line), but not across the threshold of triggering protein synthesis (θ_{pro} , dashed green line). The total weight or synaptic efficacy (orange) is the sum of early- and late-phase weight. Averaged over 100 trials; error bands show the standard deviation. The late-phase weight has been shifted for graphical reasons (cf. “Methods” section).

after the learning stimulus to analyze the short-term dynamics and after ~ 8 h to investigate the long-term effects of the STC mechanisms.

The learning stimulus consisted of three subsequent pulses of 0.1 s each, strongly activating a random subset of neurons. In experiments, strong tetanus stimuli of ~ 100 Hz are used to evoke late-phase synaptic potentiation^{18,35,51}. To resemble this, we applied stimulation of similar strength via 25 putative input neurons. A necessary consequence of this strong input is the fact that during stimulation, the stimulated neurons spike at their maximum. As expected, the stimulus caused tremendous changes of the synaptic efficacy of diverse synapses in the network (compare Fig. 3a, b). Synapses associated with the stimulated neurons (first 150 neurons Fig. 3a–c) mainly experienced LTP (red). The synapses between stimulated neurons (black box in Fig. 3a–c) are strengthened particularly, indicating the correct formation of a cell assembly. By contrast, synapses between non-stimulated neurons underwent LTP as well as LTD (blue). After 8 h, the synaptic changes between non-stimulated neurons and, thus, with the cell assembly remain (Fig. 3c). To validate that the formed cell assembly encodes a memory, next, we tested the ability of recall. For this, we applied a recall stimulus that activates for 0.1 s 50% of the neurons that were stimulated by the learning signal, and analyzed the resulting spread of activation within the network (Fig. 3d, e). The externally stimulated neurons (“as”) have the highest activity. By the strong recurrent connections in the cell assembly, the average activity of the non-stimulated neurons in the cell assembly (“ans”) is significantly higher than the activity of the remaining non-stimulated neurons (“ctrl”). This is not the case for control stimulation applied before learning. In other words, the activity of the recall stimulus spreads via the stimulated neurons to the other cell assembly neurons and yields a type of pattern completion or recall (in the literature sometimes also called retrieval). Please note that, under basal/

standby conditions, the mean firing rate of all excitatory neurons resembles the average value of 0.5–1.0 Hz for pyramidal cells in the hippocampus during exploratory wake states (refs. 49,50; see also Supplementary Fig. S3). We further analyzed the spread of activity by considering the mean firing rate correlations between the neuronal subpopulations (Fig. 3f). The correlations generally increase with learning and consolidation, which is in line with the previous finding of increased mean firing rates. Furthermore, we found that correlations within the cell assembly (“as” and “ans”) are larger than correlations with control neurons (“ctrl”), which again indicates functional memory recall and further leads to the expectation of more LTP for connections involving “as” and “ans” neurons. This already suggests an “active improvement” of the cell assembly, which we will investigate in a later section. On the other hand, the fact that correlations between cell assembly neurons and control neurons are also increased by recall stimulation shows that control neurons indirectly contribute to recall. This is corroborated by previous work⁵³ and by the distribution of synaptic weights, which exhibits tremendously increased weights from control to cell assembly neurons (“incoming” weights in Fig. 3b, c and Supplementary Figs. S4 and S5). In summary, the results presented in this section show that calcium-dependent synaptic plasticity and the STC mechanisms enable the encoding of memory and its maintenance for several hours in a recurrent neural network. Thereby, our findings support the idea that the STC mechanisms account for the synaptic consolidation of memories. In the next section, specific measures for memory recall will be presented.

Memory functionality depends on network inhibition and size of the representation. In the following, we investigate the influence of different parameters, such as inhibition and cell assembly size on the learning, recall, and consolidation of memory representations.

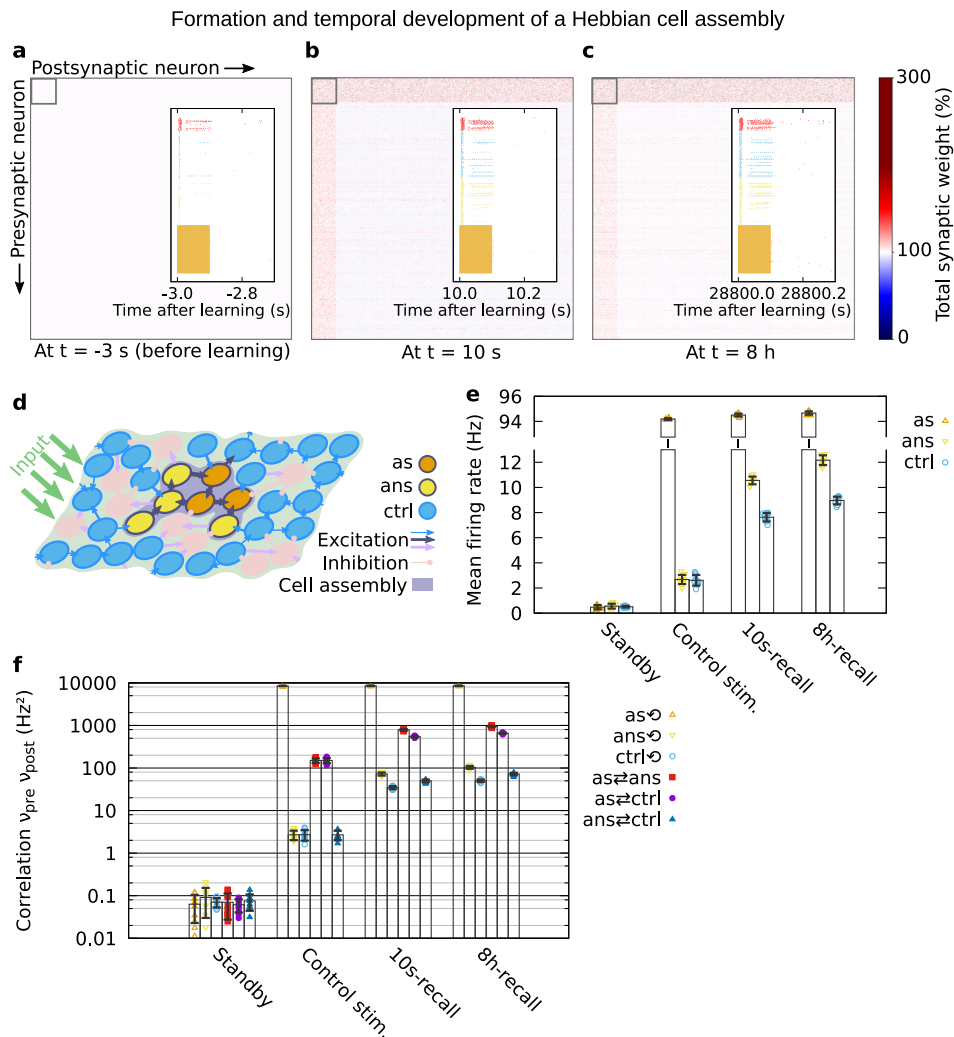


Fig. 3 Formation and temporal development of a Hebbian cell assembly and its functionality. **a-c** The matrix of total (early- plus late-phase) synaptic weights sorted by the stimulated neurons (first 150): **a** before learning, **b** -10 s after learning, and **c** -8 h after learning. The insets show the spiking during recall stimulation of the neurons in the cell assembly (colors as in **d**, **e**) and of a random 5% fraction of the neurons in the remaining excitatory (blue) and inhibitory (red) populations. **d** Schematic of the three subpopulations during recall stimulation: the fraction of externally stimulated cell assembly neurons ("as"), the fraction of cell assembly neurons that are not stimulated ("ans"), and the remaining excitatory neurons acting as control group ("ctrl"). **e** The mean firing rates of the three subpopulations defined in **d**, before learning and without recall (standby), before learning during control recall stimulation, upon recall 10 s after learning, and upon recall 8 h after learning. **f** Mean firing rate correlations (presynaptic multiplied by postsynaptic firing rate, averaged over neuron pairs) within and between subpopulations for the same protocols as in **e**. Synaptic weights, mean firing rates and mean correlations were averaged over ten trials. Error bars show the standard deviation. Parameters: $w_{ie}/h_0 = 4$, $w_{ii}/h_0 = 4$.

In general, one role of inhibition in neural networks is to prevent the network activity from runaway or epileptiform dynamics. This kind of dynamics is characterized by neurons constantly exciting each other and firing at the maximum possible rate. On the other hand, if inhibition is excessively strong, neuronal activity is confined, resulting in a more or less silent network. We adjusted the level of inhibition in our network by varying the coupling strength from inhibitory neurons to excitatory neurons (w_{ie}) and the coupling strength from inhibitory to inhibitory neurons (w_{ii}). For every set of these parameter values, we simulated the network dynamics during learning and recall, as described before. At two different points in time (10 s and 8 h after learning), we evaluated the memory functionality that consists of learning, consolidation, and recall of a memory by measuring the recall quality. To measure the recall quality, we used two different quantities (cf. "Methods" section): on the one hand, the pattern completion coefficient Q describes by how much the activity in the non-stimulated part of the input-

defined cell assembly is raised during recall, as compared to the activity of the control neurons; on the other hand, the mutual information MI_v describes how similar the network activity state during recall is to the network activity state during learning. We quantitatively defined memory functionality by an average pattern completion coefficient of $Q \geq 0.03$. This criterion demands that, upon stimulation of half of the assembly neurons, the other half of the assembly be activated much stronger than the background neurons, which remain at a low activity level (cf. Fig. 3e). Please note that the values of the pattern completion coefficient appear small because we normalize by the activity of the stimulated neurons (cf. Eq. (17)).

High values of the $I \rightarrow I$ coupling strength together with low values of the $I \rightarrow E$ coupling strength imply a low level of inhibition, which impedes memory functionality in our network model (see Fig. 4a, c for the recall performance 10 s after learning and Fig. 4b, d for 8 h after learning). This impairment goes along with the runaway dynamics discussed before, as indicated by the

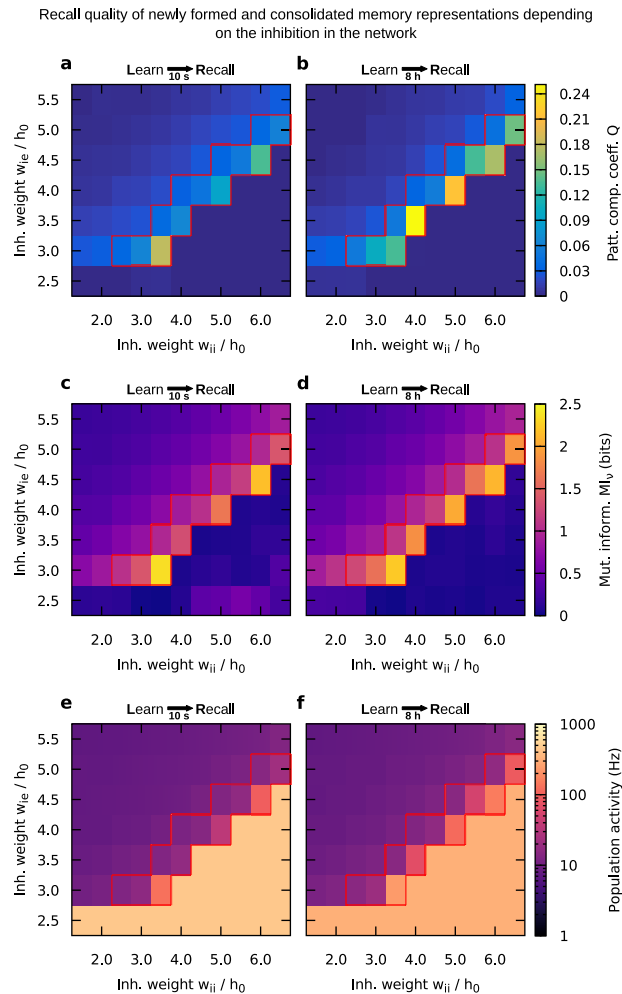


Fig. 4 Quality of the recall 10 s and 8 h after learning as a function of the $I \rightarrow E$ (w_{ie}) and $I \rightarrow I$ (w_{ii}) coupling strengths. Sufficient memory functionality is found within a certain regime, marked by a red box ($Q(10\text{s-recall}) \geq 0.03$). Two measures of recall quality are shown: **a, b** the pattern completion coefficient Q (with nonsignificant values set to zero, see “Methods” section); **c, d** the mutual information MI_v between the neuronal activities in the network during learning and during recall. **e, f** For comparison, the neuronal activity averaged over the whole excitatory population is shown. All three observables were averaged over ten trials. Parameters: $n_{CA} = 150$, $I_0 = 0.15$ nA.

extreme level of population activity in this parameter regime (Fig. 4e, f). In general, if a network is in such an “epileptiform” state, a recall stimulus does not exclusively activate the neurons that belong to the cell assembly - it also activates a large fraction of control neurons, overshadowing memory recall. On the other hand, low values of the $I \rightarrow I$ coupling strength together with high values of the $I \rightarrow E$ coupling strength lead to extensive levels of inhibition, suppressing the neuronal activity during recall. In other words, the activity induced by a recall stimulus will immediately be suppressed by the high level of inhibition, also impeding memory recall. As a result, the level of inhibition has to be within a specific regime to enable learning, consolidation, and successful recall of memories (indicated by the red box; $Q(10\text{s-recall}) \geq 0.03$). This regime is characterized by medium levels of population activity. The functionality is relatively stable given variations in the mean background current I_0 (Supplementary Fig. S6), while also the mean firing rate only weakly depends on the mean background current (Supplementary Fig. S3b).

Furthermore, the recall quality remains relatively high at low learning and recall stimulus frequencies, except for very low frequencies, where the memory functionality ceases (Supplementary Fig. 7). This resilience is partially due to the number of 25 putative input neurons. In summary, the level of inhibition within the described regime of functionality seems to be sufficient to prevent the overly activation of control neurons, while it remains low enough to allow the desired activation of the non-stimulated neurons within the cell assembly. Please note that such a regime is related to the network state of loosely balanced excitation and inhibition (ref. 54; also see “Discussion” section).

The regime of memory functionality is the same either 10 s or 8 h after providing the learning stimulus. However, the higher values of Q and MI_v after 8 h compared to the 10 s case indicate a positive influence of long-term dynamics on the memory functionality. We further investigate and discuss this result in the next section.

As further parameter, we examined the influence of the size of the cell assembly on the memory functionality (Fig. 5a, b). We controlled the size by varying the number of neurons being the subgroup that is stimulated by the learning stimulus. Following our definition of memory functionality, requiring that the coefficient $Q \geq 0.03$, we found that learning and recall is only possible if the cell assembly is large enough. In the following, we will focus on a particular set of parameter values for the inhibition ($w_{ie}/h_0 = 4$, $w_{ii}/h_0 = 4$). All derived conclusions apply to all sets within the specific regime of inhibition discussed before (red box in Fig. 4). For small cell assemblies (here ~ 100 neurons), the group of neurons is too small to exhibit functional pattern completion (threshold indicated by the dotted red line in Fig. 5a, b). For large cell assemblies (here >500 neurons), the activity of the cell assembly becomes self-sustained. This means that after learning the neurons within the cell assembly stay active, preventing the typical dynamics of memories we are looking for. Moreover, the measures of the recall quality exhibit local maxima. The occurrence of these maxima cannot be explained by the relationship between the mean firing rate and the cell assembly size, because this relationship is strictly monotonic and does not feature any maximum (Supplementary Fig. S3a). Therefore, we reason that the maxima emerge from the additional stimulation by the recall cue. Finally, similar to Fig. 4, the pattern completion coefficient and mutual information become higher 8 h after learning compared to 10 s after learning for a large range of cell assembly sizes, which will be examined further in the next section.

Consolidation improves memory recall. Comparing the recall quality of the cell assembly 10 s after learning with the recall quality 8 h after learning for different paradigms (Figs. 4 and 5a, b), we found that 8 h after learning the system generally exhibits an improved recall quality. In other words, the specific state of the cell assembly after 8 h, resulting from the interplay between calcium-dependent synaptic plasticity and the STC mechanisms, seems to facilitate recall. To elucidate the magnitude of the improvement effect, we computed the relative gain in recall quality between the state 10 s after learning and the state 8 h after learning, and present results for the particular inhibition setting that we chose before (Fig. 5c, d). It becomes obvious that improvement in recall quality can occur by $>200\%$ with respect to the pattern completion coefficient, and by as much as 30% with respect to the mutual information.

To test the robustness of the improvement effect across the specific inhibition regime identified before, we averaged MI_v and Q over the range of parameter settings of this regime and calculated the relative gain in recall quality (Fig. 5e, f). For the

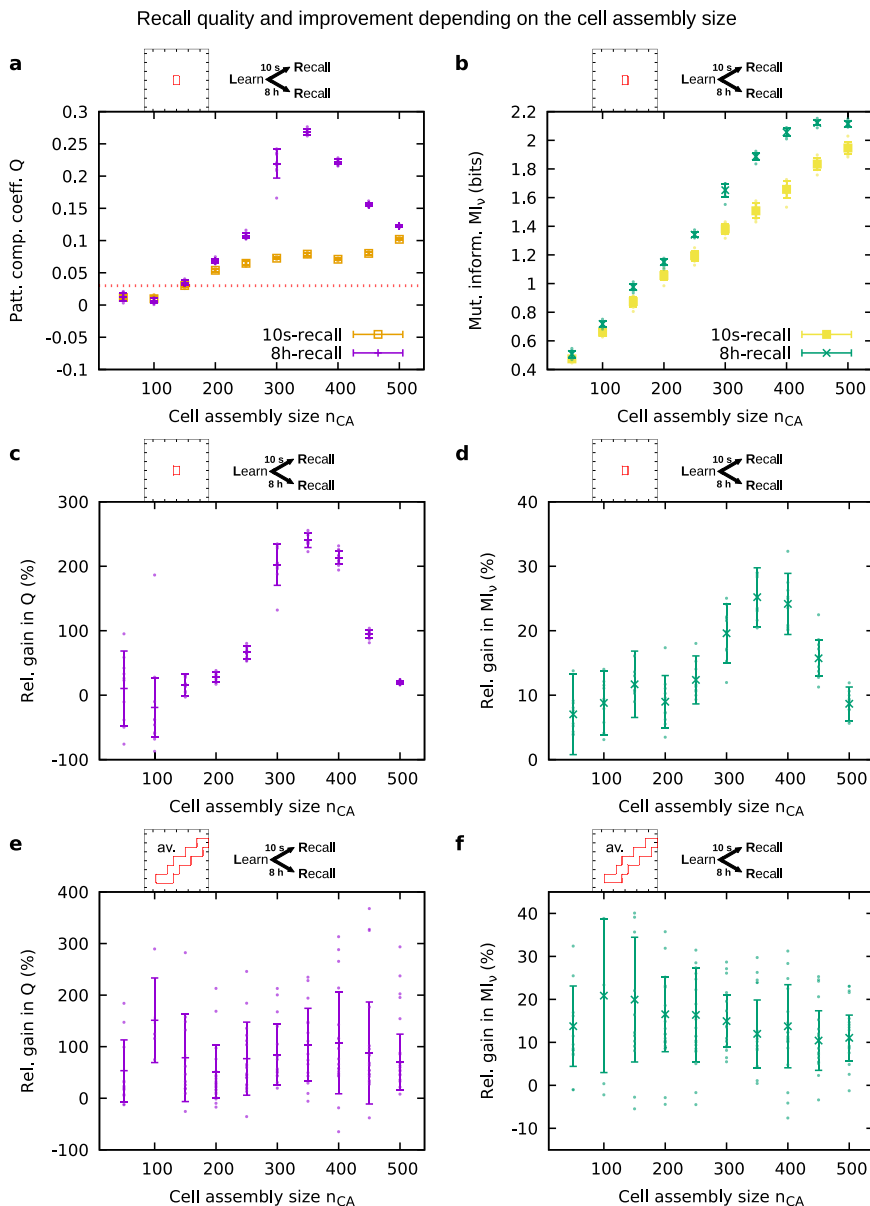


Fig. 5 Recall quality 10 s and 8 h after learning and resulting relative gain as a function of the cell assembly size. **a** Pattern completion coefficient 10 s (orange) and 8 h (purple) after learning. The dotted red line indicates the threshold for memory functionality ($Q \geq 0.03$). **b** Mutual information of the neuronal activities 10 s (yellow) and 8 h (green) after learning. **c** Relative gain in pattern completion coefficient between 10 s and 8 h after learning. **d** Relative gain in mutual information of the neuronal activities between 10 s and 8 h after learning. **a–d** Averaged over ten trials; parameter values: $w_{ie}/h_0 = 4$, $w_{ii}/h_0 = 4$. **e** Relative gain in pattern completion coefficient, **f** relative gain in mutual information, averaged over the mean gain values (from ten trials) of all inhibition parameter sets that yielded functional memory for the respective cell assembly size (i.e., the sets with $Q(10s\text{-recall}) \geq 0.03$, for size 150 cf. the red boxes in Fig. 4). Error bars indicate in **a, b**, the standard deviation across ten trials, in **c, d**, the error propagated from **a, b**, and in **e, f**, the error propagated from the standard deviations (from ten trials) of the functional parameter sets.

chosen inhibition setting $w_{ie}/h_0 = 4$, $w_{ii}/h_0 = 4$ (Fig. 5c, d), as well as for the averaged results (Fig. 5e, f), we observed a positive gain across all cell assembly sizes. Positive gain means that 8 h after learning the performance was better than 10 s after learning. Thus, for a wide range of parameter settings, the passage of time yields an improvement of the recall quality.

What are the underlying principles that lead to this improvement of the recall quality? We could identify two processes, both being related to the STC mechanisms: an active and a passive improvement.

The *active improvement* is related to the dynamics of the early-phase weights. The recall stimulus provided 10 s after learning only leads to minor variations of the average early-phase

weight in the cell assembly (dashed red line at “R” in Fig. 6a). By contrast, 8 h after learning the recall stimulus triggers a substantial increase of the average early-phase weight which in turn results in a stronger total synaptic weight (dashed red and orange line at “R” in Fig. 6b). Thus, 8 h after learning the average total synaptic weight of the cell assembly increases during the recall, which improves the recall performance (Fig. 5). By comparing the state of the neural network between both time points, we find that the average early-phase weight before the 10s-recall resides on a much higher level than before the 8h-recall (Fig. 6c). This difference in early-phase weight before recall stimulation could explain the different dynamics of the early-phase weights during the recall. Considering the mathematical

Synaptic weights during memory formation, consolidation and improvement

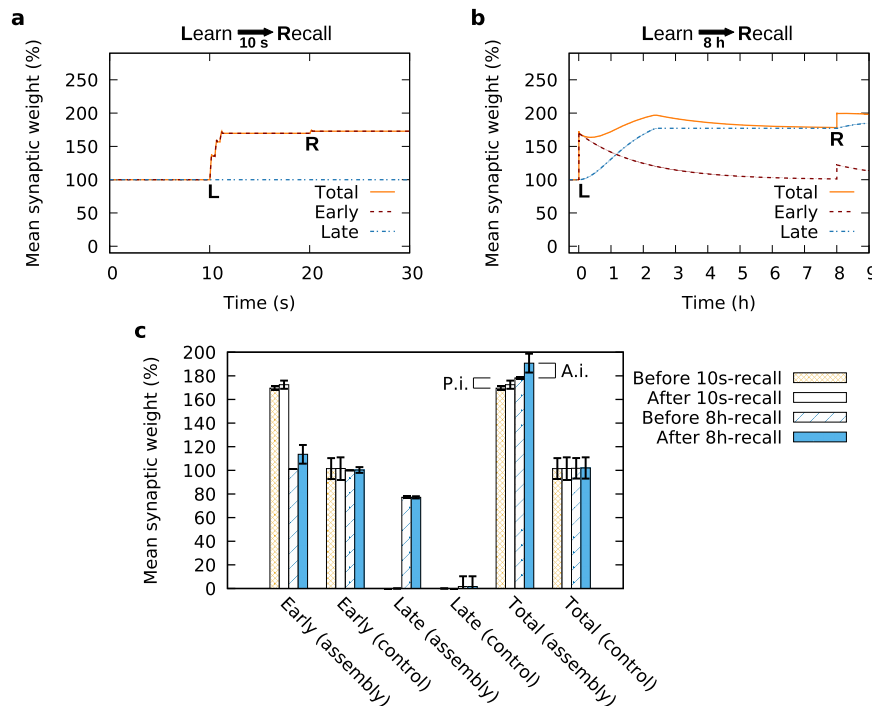


Fig. 6 Synaptic dynamics related to memory formation, consolidation and improvement. **a** During the first seconds after the learning stimulus (“L”), the average early-phase weight (red) of the synapses connecting the stimulated neurons increases, while the average late-phase weight remains constant (blue). A recall stimulus (“R”), provided 10 s after the learning stimulus, does not exert a substantial effect on the synaptic weights. **b** Several hours after learning, the average early-phase weight decays, while the late-phase increases such that the average total synaptic weight remains on a high level. Providing a recall stimulus 8 h after learning triggers an increase of the average early-phase weight and, thus, of the total synaptic weight. **a, b** Averaged over ten trials; the error bands (representing the standard deviation) are too small to be visible. **c** Mean early- and late-phase weights within the assembly and within the non-assembly (control) population immediately before and immediately after the 10s and 8h-recall. A.i. active improvement component (difference between solid blue and blue hatches); P.i. passive improvement component (difference between orange grating and blue hatches). Data from one sample network. Error bars show the standard deviation across the subpopulation. See Supplementary Figs. S4 and S5 for detailed distributions of the underlying data. Parameter setting: $w_{ie}/h_0 = 4$, $w_{ii}/h_0 = 4$, $n_{CA} = 150$.

formulation of the model, one can see that the change of the early-phase weight depends on the distance of the actual early-phase weight h from its initial or equilibrium value h_0 . Hence, larger changes occur if the early-phase weight is closer to the equilibrium state, while the changes remain smaller if the early-phase weight is close to its maximum value. Thus, the learning stimulus “pushes” the early-phase synaptic weight into a regime in which the subsequent recall cannot trigger further strengthening. However, with the passage of time the early-phase weight decays (while the late-phase weight increases) until it reaches the vicinity of its initial value (Fig. 6b, c). In this regime, a recall stimulus can again trigger an increase of the early-phase weight, supporting pattern completion. The detailed weight distributions for all cases presented in Fig. 6c and additional data revealing the weights between subpopulations of the network are shown in Supplementary Figs. S4 and S5. To further scrutinize the relation between the early-phase dynamics during recall and the improved recall quality, we performed simulations in which we switched off or blocked early-phase plasticity after learning. Comparing the resulting recall performances with the simulations with early-phase plasticity (Fig. 7), for both measures Q and MI_v , we did not find an influence of the blockage during 10s-recall but during 8h-recall. These results further support our finding that the dynamics of the early-phase weights within the cell assembly are one essential part underlying the improvement of the recall quality.

The other part of the improvement of the recall quality is related to the dynamics of the late-phase weights within the cell

assembly. We refer to this part as *passive improvement*. As expected, 8 h after learning the STC mechanisms yield a decrease of the average early-phase weight (red line in Fig. 6b) accompanied by an increase of the average late-phase synaptic weight in the assembly (blue line) that indicates the process of synaptic consolidation. However, if we compare the average total synaptic weight within the assembly before the 10s-recall with the one before the 8h-recall (Fig. 6), we identify an increase that suggests a second component underlying the improvement of recall quality. This is also indicated by the relative gain in Q and MI_v without early-phase plasticity (Fig. 7). Hence, although the dynamics of the early-phase weights (active improvement) explains the gain in recall quality to a large extent, there is a remaining part that is related to the dynamics of the late-phase weights (passive improvement).

Parameter dependency of the passive improvement. We have found that the mean total weight of a cell assembly can increase over time, and refer to this phenomenon as passive improvement (cf. Fig. 6c). This effect is elicited by the mechanisms of STC and occurs if the mean normalized late-phase weight $\bar{z} \cdot h_0$ after 8 h becomes higher than the mean early-phase weight \bar{h} after learning. To investigate and predict the circumstances under which this effect occurs, namely, different settings of late-phase-related constants, we considered an analytical approach that we present in the following.

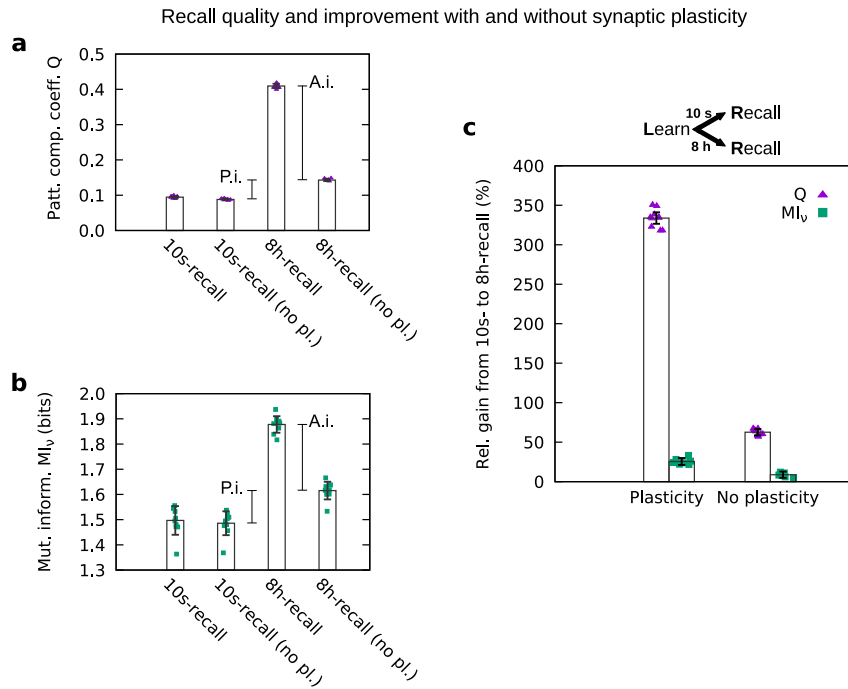


Fig. 7 Recall quality measured for recall 10 s and 8 h after learning with and without early-phase synaptic plasticity during recall. The effect of early-phase synaptic plasticity on the total improvement is significant (compare 8h-recall with 8h-recall no pl.: A.i. active improvement), but it does not cover the complete level of improvement (compare 10s-recall with 8-h recall no pl.: P.i. passive improvement). **a** Pattern completion coefficient Q; **b** mutual information MI_v ; and **c** relative gain in Q and MI_v from 10s-recall to 8h-recall. All observables averaged across ten trials. Error bars indicate standard deviation across the ten trials in **a, b** and the propagated error in **c**. Parameter setting: $w_{ie}/h_0 = 4$, $w_{iv}/h_0 = 4$, $n_{CA} = 350$ (value of the maximum in Fig. 5c, d).

To investigate the parameter dependency of consolidation and improvement of a cell assembly, we analytically solve the linear first-order differential equation describing the dynamics of late-phase LTP (cf. Eq. (14)) with a variable coefficient introduced by the time-dependent amount of proteins (Eq. (15)). Since L-LTP is vastly predominant between cell assembly neurons, we neglect here the L-LTD dynamics.

Thus, the analytical expression for the mean late-phase weight after time t after learning in the case of persistent tags and protein synthesis is:

$$z_f(t) = 1 - (1 - z_0) \cdot \exp\left(-\frac{\tau_p(\alpha - p_0) \cdot e^{-\frac{t}{\tau_p}} + \alpha t - \alpha \tau_p + p_0 \tau_p}{\tau_z}\right) \quad (1)$$

depending on the protein time constant τ_p , the late-phase time constant τ_z , the initial protein amount p_0 , the initial late-phase weight z_0 , and the protein synthesis rate α . Note that this equation only holds if tags have been set and as long as they have not vanished, which we will address later. This solution can be further simplified under the condition that the initial late-phase weight z_0 and the initial protein amount p_0 are zero. The mean increase in late-phase weight due to the STC mechanisms is then:

$$z_s(t) = 1 - \exp\left(-\frac{\alpha(t + \tau_p \cdot e^{-\frac{t}{\tau_p}} - \tau_p)}{\tau_z}\right) \quad (2)$$

For Eq. (2), we considered that the synapses within the cell assembly are always tagged, triggering changes of the late-phase weights. However, after learning the early-phase weight decays (Fig. 6b) and falls at a certain point in time below the tag-sufficient threshold. Thus, first, we have to calculate the decay of the mean early-phase weight and, then, use it to determine at what time the tag will have vanished. The average decaying early-

phase weight follows

$$h_d(t) = (\tilde{h} - h_0) \cdot \exp\left(-0.1 \frac{t - t_{al}}{\tau_h}\right) + h_0 \quad (3)$$

depending on the mean early-phase weight after learning \tilde{h} , the time after learning t_{al} , the initial weight h_0 , and the early-phase time constant τ_h . The time t_{al} is a time after learning (for instance, 10 s) at which \tilde{h} , the mean learning-induced increase in early-phase weight, is measured. Setting $h_d(t)$ to the value of the tagging threshold $\theta_{tag} + h_0$ yields the point in time t_{tag} at which the synaptic tags will have vanished on average:

$$t_{tag} = 10 \tau_h \cdot \ln\left(\frac{|\tilde{h} - h_0|}{\theta_{tag}}\right) + t_{al} \quad (4)$$

The synaptic tags typically vanish before the synthesis of new proteins stops and, thus, t_{tag} determines the end of late-phase changes, such that the average late-phase weight is described by

$$z_{st}(t) = \begin{cases} z_s(t) & \text{if } t \leq t_{tag}, \\ z_s(t_{tag}) & \text{if } t > t_{tag}. \end{cases} \quad (5)$$

Hence, for parameter sets yielding $t_{tag} < 8$ h (cf. Eq. (4)), the mean late-phase weight before the 8h-recall is the same as by the time the tags vanished (see also Fig. 6b, blue line):

$$\tilde{z} = z_s(t = t_{tag}). \quad (6)$$

In Fig. 8a, we plot the mean weights within the cell assembly, using our numerical results for early-phase LTP during learning and recall to compute the late phase via the analytical function in Eq. (5) and the decay of the early-phase weight as detailed in Eq. (3). As expected, we find that this analytical approach predicts very well the mean weight dynamics of our numerical simulations (dashed gray line in Fig. 8a, cf. Fig. 6b).

Analytical calculation of the long-term mean weight dynamics

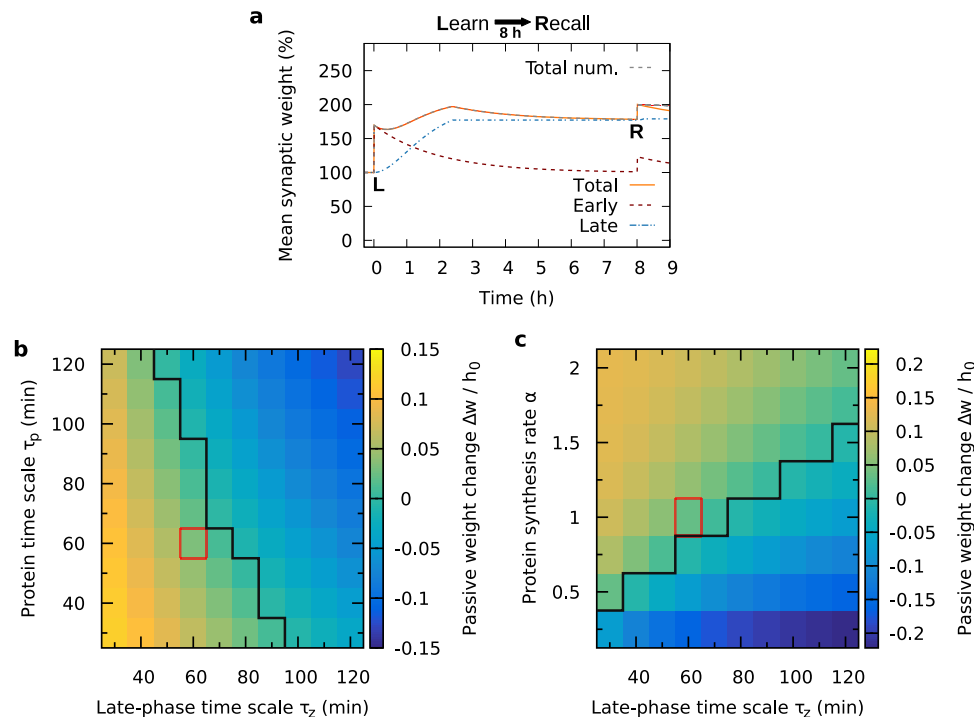


Fig. 8 Analytical investigation of the long-term weight dynamics and passive improvement depending on late-phase time constants. **a** The early-phase values immediately after learning (“L”) and after recall (“R”) were taken from the average over numerical simulations (Fig. 6b) and inserted into the analytical equations for the late-phase dynamics (Eq. (5)) and the early-phase decay (Eq. (3)). The curves are in very good match with the simulated results, the total weight of which is shown here for comparison by the dashed gray line (cf. Fig. 6b). **b, c** Varying the time constants for late-phase dynamics τ_z and protein amount τ_p (**b**), as well as the protein synthesis rate α (**c**), shows that for slower time scales and lower synthesis rate, the passive weight change becomes negative, i.e., there is a passive deterioration instead of improvement. The black separatrix line demarcates the two regimes of improvement and deterioration. The red boxes indicate the parameter values used in our numerical studies.

When we compare the mean total weight 8 h after learning $w(t = 8 \text{ h})$ with the mean total weight 10 s after learning $w(t = 10 \text{ s})$, we obtain an expression for the passive weight change realized by the STC mechanisms, thus, of the passive improvement:

$$\Delta w = w(t = 8 \text{ h}) - w(t = 10 \text{ s}) = \tilde{z} \cdot h_0 - \tilde{h}. \quad (7)$$

If $\Delta w > 0$, the system shows a passive improvement with the passage of time, which is given for a wide range of parameter values. For instance, by considering different values of the protein synthesis parameters, namely the time constant of the protein amount τ_p (Fig. 8b) and protein synthesis rate α (Fig. 8c), depending on the time scale of the late-phase dynamics τ_z , we can determine the influence of protein synthesis on the passive improvement. We find that, if the protein time scale becomes too high or the synthesis rate becomes too low, the passive weight change switches from improvement to deterioration. However, the protein dynamics can be much slower than in our numerical simulations (red box) and still the STC mechanisms yield an improvement. For the protein synthesis rate, there is just as well a wide range of values that gives rise to improvement. Thus, the encountered improvement effect is robust to parameter variations.

Our analytical results lead to the following predictions: if the time scale of the protein dynamics is manipulated, the resulting memory behavior should switch between passive improvement and deterioration. In addition, manipulating the speed of signaling cascades that are involved in late-phase LTP should have a similar effect. Taking this into account, our predictions can be useful to narrow down the set of possible proteins and processes involved in STC.

Intermediate recall further amplifies memory improvement.

There are several psychological studies that investigate hypermnesia/improvement by considering the memory strength after multiple recalls^{55–57}. Therefore, we also investigated the impact of an intermediate recall on the memory dynamics. For this, we computed the gain in the pattern completion coefficient Q and in the mutual information MI_p between 10s-recall and 8h-recall after applying an additional, intermediate recall stimulus to randomly drawn neurons.

We varied the time of occurrence of this intermediate stimulus (Fig. 9). The gain in recall quality for early intermediate recall (minutes after learning) shows little difference to the gain without intermediate recall (data point at time zero). For late intermediate recall, the gain reaches values that are much higher compared to the case without intermediate recall. Hence, additional recall improves the recall quality even further, which is consistent with the experimental findings^{55–57}.

Discussion

In this study, we developed a recurrent network model to show that the mechanisms of STC^{15,18–20} provide a biological basis for encoding, consolidation, and recall of memories. We found that these mechanisms also cause an improvement in the recall quality of memories, which is robust across a large space of parameter settings. While the possibility of such improvement was proposed previously based on an abstract plasticity model featuring multiple timescales^{40,42}, we show that memory improvement can arise from the STC mechanisms. Previous theoretical studies of STC focused on molecular pathways¹²,

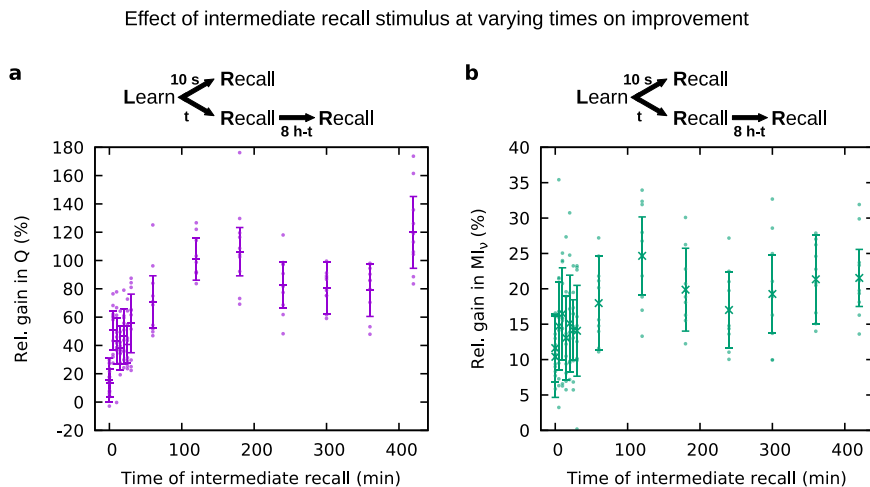


Fig. 9 Relative gain in recall quality between 10 s and 8 h after learning, affected by an intermediate recall stimulus at varying times. **a** Gain in pattern completion coefficient Q ; **b** gain in mutual information MI_q . Parameter values: $w_{ie}/h_0 = 4$, $w_{ii}/h_0 = 4$, $n_{CA} = 150$. Averaged over ten trials. Error bars indicate the error propagated from the standard deviations across ten trials for both 10s-recall and 8h-recall. The data points at time zero show the case without intermediate recall (as in Fig. 5c, d).

single synapses^{15,20,27,28}, and feed-forward networks²⁸, and thereby provided fundamental insights into the processes underlying the synaptic consolidation of memories. However, to the best of our knowledge, there have not yet been studies targeting the effects of STC in recurrent networks, which are essential for the encoding of memories. We set out to close this gap and we were able to characterize emergent effects that arise from the conjunction of STC with strongly recurrently connected groups of neurons (cell assemblies).

Detailed models describing the molecular dynamics underlying synaptic plasticity and STC have been shown to be compatible to and to offer a complementary view on simpler statistical models^{12,13,20,27,58}. We use a model for synaptic plasticity based on calcium dynamics because this approach captures a wide range of experimental findings, including spike-timing-dependent phenomena and rate-coding behavior^{13,16,30–33,37–39}. For STC, we use a model based on generalized plasticity-related proteins that account for the crucial aspects of tagging, capture, and cross-tagging^{15,19,20,34–36}. Thereby, our model contains the essential features of a biologically more detailed model, while still being computationally tractable.

By varying the size of the cell assembly, we found different recall dynamics of the system. We found that there is a lower bound to the size, below which the amplification of recall stimulation does not suffice for functional recall. On the other hand, large cell assemblies show attractor behavior, meaning that after the application of a recall stimulus they become fully activated and stay activated. Investigating this attractor regime is beyond this study. Nevertheless, considering attractor dynamics in our model could reveal interesting implications, since long-term memory representations exhibiting attractor dynamics can serve as working memory^{59,60}, possibly in conjunction with additional transient dynamics⁶¹. Varying the inhibitory synaptic weights, we found a regime of parameters yielding functional memory dynamics. This regime seems to correspond to “loosely balanced” network states, which are characterized by a dynamic equilibrium of excitation and inhibition⁵⁴. In contrast to that, “tightly balanced” network states feature inhibition that closely follows excitation, and in some cases seem to enable more efficient coding. By introducing inhibitory plasticity^{62,63}, our network could possibly enter a tightly balanced state. This would increase the complexity of our model tremendously, but could be subject to future studies on more efficient memory encoding.

Synaptic plasticity such as LTP is widely considered to be the main mechanism that underlies memory, as it is expressed by the synaptic plasticity and memory hypothesis^{6,9}. LTP of synapses has been subdivided into three different types: LTP1, which depends on stimulation only, LTP2, which depends on translation of existent mRNA, and LTP3, which depends on transcription in the soma^{9,64,65}. LTP2 and LTP3 are often subsumed as late-phase LTP, whereas LTP1 is called early-phase LTP^{9,18}, which paradigm is followed by our study. Similar phenomena and processes as the ones discussed for LTP are found for LTD^{9,12,35}. In addition to synaptic plasticity, there are hints to other, cell-intrinsic mechanisms that might be relevant for the storage of memory⁹, such as noncoding RNAs that produce learning-related epigenetic changes in neurons⁶⁶. However, the potential effects of such non-synaptic memory mechanisms on the results of our study and on memory consolidation in general remain unknown and require further investigations.

Following their encoding, memories can become consolidated to last for hours, days, or even years, depending on conditions like strength of the learning stimulus and neuromodulation^{1,24,65}. In principal, one can distinguish two different paradigms related to memory consolidation. On the level of brain areas, systems consolidation describes the transfer of newly formed memories, mainly from the hippocampus to the neocortex^{1,24}, as it was first discovered in the case of the patient H.M.⁶⁷. This type of consolidation is related to sleep and rest^{50,68,69}. On the other hand, there is synaptic consolidation, which denotes the in-place stabilization of changes in the strength of synaptic connections^{24,26}, and thereby is a synonym for LTP2 and LTP3, or late-phase LTP as discussed before⁹. Blocking of hippocampal LTP has been shown to prevent long-term memory during wake in the first hours after learning^{67,70}, which is why the hippocampus seems to be the central region for this first stage of memory consolidation. In our study, we do not consider sleep- or rest-dependent consolidation, which would require the presence of activity patterns like shape-wave/ripples, spindles, or slow oscillations^{26,49,50}. Instead, we target the encoding and the in-place synaptic consolidation of memories. This occurs for instance during exploratory wake state in hippocampal networks^{24,26,70}. Although our model resembles some characteristics of hippocampal networks, it could describe a network in any other brain region that features similar processes. Moreover, extending our model by sleep-related activities^{69,71} could yield interesting

insights into the interplay between synaptic and systems consolidation.

Sometimes it is being suggested to use the term cellular consolidation instead of synaptic consolidation^{1,19}, since the processes involved are not only located at the synaptic site. This is mostly due to the fact that mRNA and proteins are synthesized in the soma, from where they are transported to the dendrites and spines^{1,19,20,65}. Nevertheless, there can also be local protein synthesis in the dendrites^{72–75}, which could confine the here identified protein-dependent dynamics of consolidation and improvement to specific dendritic branches of a neuron. However, due to synaptic clustering⁷⁶, local protein synthesis would not necessarily yield different results as compared to our model.

The most important finding of our study is that for many parameter settings, the quality of recall 8 h after learning is much better than the quality of recall 10 s after learning. In psychological literature, such an increase in recall quality over time is referred to as memory improvement or hypermnesia⁷⁷. It has been found particularly, but not exclusively, in picture memory^{56,57,77}. In our simulations and analyses, we found the improvement effect to occur already at the very first recall attempt, while in psychological experiments the effect of improvement has mostly been measured over the course of several recall attempts. Our model accounts as well for improvement by multiple recalls, as we showed using a protocol with an intermediate recall stimulus. Nevertheless, there are experiments indicating that recall can already be improved in the first attempt⁷⁷. It would be desirable to have more experimental data on very early recall, as well as on recall after 8 h without previous recall.

Our model explains another interesting, seemingly fundamental feature of memory consolidation. As studies on positive effects of memory disuse have proposed^{78,79}, learning will be most powerful after a break, when the storage strength is still quite low and the retrieval strength has again decreased. Attempts to retrieve will then result in a strong increase in storage strength. If the retrieval strength is still high, the gain in storage strength upon this (“easy”) retrieval will be low. This theory seems to be partially consistent with our results, considering that the storage strength correspond to the late-phase synaptic weight, and retrieval strength to the early-phase synaptic weight. In our model, increases in early-phase weights upon stimulation are much larger if the early-phase weight is low before the stimulation than if it is high. Since increases in early-phase weight lead to changes in late-phase weight, the gain in late-phase weight (i.e., presumably, the storage strength) indeed inversely depends on the early-phase weight (retrieval strength) before the stimulation. Nevertheless, further investigations would have to resolve how our model could match the psychological finding that retrieval at small retrieval strength should take long^{78,79}, while at the present our model exhibits fast recall even in the case of low early-phase weights.

Behavioral tagging is a phenomenon that could be the behavioral analog of synaptic tagging, describing the finding that the memory of a weak input perceived around the same time as strong novel stimulation becomes consolidated along with the memory of the strong stimulus^{80–82}. While by now, there is plenty of evidence relating behavioral tagging to synaptic tagging, the knowledge gap is not yet closed²². Using their theoretical model of a feed-forward network, Ziegler and colleagues²⁸ provided a connection between STC mechanisms and behavioral tagging, focusing on an inhibitory avoidance paradigm. For this, they considered dopamine modulation to model novelty. By extending our model by such dopamine modulation, for instance via the protein synthesis threshold, more experimental data could be matched to provide further evidence for the relatedness of behavioral tagging and synaptic tagging.

Our model predicts an active and a passive improvement of memories by the STC mechanisms for a wide range of parameter values. In the following, we discuss how these predictions can be verified in experiments on the behavioral level, on the network level, and on the synaptic level. At the behavioral or psychological level, our findings can be tested with subjects that need to learn a set of items, like words or pictures, and then recall the items after a very short time (~10 s). The performance of this recall should then be compared with the performance of the same subjects in a similar task but with other items, and recall after 8 h. Ideally, to be comparable to our results, there should not be any attempt to recall during the 8 h, which could be hard to manage for the subjects. However, at least trying to avoid intermediate recall would provide some new insights, as compared to previous psychological studies that were based on intermediate recall^{55–57}. In *in vitro* networks, multielectrode arrays (MEAs) can be used to stimulate many neurons at the same time, as well as to measure their activity⁸³. For our purposes, an MEA could be used to trigger plasticity, forming a strongly interconnected cell assembly. After the formation, a partial recall stimulus should be applied and the resulting activity be measured. The activity during 10s-recall (10 s after learning) and during 8h-recall (8 h after learning) can then be compared, as it was shown in Fig. 3e. If the activity in the cell assembly following 8h-recall is higher, then there will be experimental evidence for memory improvement. Another promising approach to test the memory improvement at the network level would be to use optogenetic stimulation in combination with activity measurements through calcium imaging, which is an established method that is very suitable for *in vivo* experiments^{84,85}, and can be tuned to deliver precise learning and recall stimulation^{86–88}. Our study also yields predictions for the synaptic level. To test these, first, synaptic potentiation has to be induced applying a strong “learning” stimulus to a nerve fiber. Later application of a shorter “recall” stimulus to the fiber should then cause a response that depends on the time that has passed since learning. Following our predictions, the response, which can be measured as a relative field excitatory postsynaptic potential (often abbreviated %fEPSP), should be larger 8 h after learning than 10 s after learning, corresponding to the mean total synaptic weight shown in Fig. 6. Furthermore, after the application of two “recall” stimuli, the response should even be higher, as we showed in the section on intermediate recall. Finally, in any experiment, blocking the dynamics that lead to early-phase plasticity should diminish the improvement effect significantly, because we predict that active improvement is triggered by the early-phase dynamics (cf. Fig. 7c). Such experiments could be realized by using NMDA receptor antagonists or by blocking exocytosis before the presentation of a recall stimulus. In addition, blocking or slowing down late-phase-related signaling cascades and protein dynamics should, beyond a certain level, prevent passive improvement and thereby also diminish the total improvement effect (cf. Fig. 8b, c).

Please note that for several of the potential extensions of our model discussed above, it would be useful to improve the computational efficiency of the numerical simulation. For that, it is very promising to implement our network model on neuromorphic hardware^{89,90}. Neuromorphic hardware enables the simulation of larger networks and thereby the storage of many cell assemblies. In this way, storage capacity and the interference between cell assemblies could be investigated. The neuromorphic approach would not only facilitate scientific investigations but, due to its good performance and energy efficiency^{90,91}, also offer great opportunities for the technical application of our model. Implemented on neuromorphic hardware, our model could be used for fast, energy-efficient self-improvement of information storage after a few presentations. In conclusion, our theoretical model provides a further piece of evidence that the STC

Table 1 Values were used as given in this table, unless stated otherwise.**Parameters for neuron and static network dynamics**

Symbol	Value	Description	Refs.
Δt	0.2 ms	Duration of one time step for numerical computation	
τ_{mem}	10 ms	Membrane time constant	92,96
τ_{syn}	5 ms	Synaptic time constant, also for external background current	92,96,99
$t_{\text{ax,delay}}$	3 ms	Axonal spike delay	92,100
t_{ref}	2 ms	Duration of the refractory period	96,101
R	10 M Ω	Membrane resistance	96
V_{rev}	-65 mV	Reversal (equilibrium) potential	96
V_{reset}	-70 mV	Reset potential	96
V_{th}	-55 mV	Threshold potential to be crossed for spiking	96
σ_{wn}	0.05 nA s ^{1/2}	Standard deviation for Gaussian noise in external background current	
I_0	0.15 nA	Mean of the external background current	
N_e	1600	Number of neurons in the excitatory population	
N_i	400	Number of neurons in the inhibitory population	
p_c	0.1	Probability of a connection existing between two neurons	48
h_0	0.420075 nC	Initial excitatory \rightarrow excitatory coupling strength	15
w_{ei}	$2h_0$	Excitatory \rightarrow inhibitory coupling strength	
w_{stim}	h_0	Coupling strength of synapses from putative input neurons	
N_{stim}	25	Number of putative input neurons for stimulation	
f_{stim}	100 Hz	Frequency of learning/recall stimulation from putative input neurons	15,51
r	0.5	Fraction of assembly neurons that are stimulated to trigger recall	

Table 2 Values were used as given in this table, unless stated otherwise.**Parameters for synaptic plasticity**

Symbol	Value	Description	Refs.
$t_{c,\text{delay}}$	0.0188 s	Delay of postsynaptic calcium influx after presynaptic spike	13
c_{pre}	1 (0.6)	Presynaptic calcium contribution (network adjustment)	13,15,95
c_{post}	0.2758 (0.1655)	Postsynaptic calcium contribution (network adjustment)	13,15,95
τ_c	0.0488 s	Calcium time constant	13,15
τ_h	688.4 s	Early-phase time constant	13,15
τ_p	60 min	Protein time constant	15,20
τ_z	60 min	Late-phase time constant	15,20
γ_p	1645.6	Potential rate	13,15
γ_d	313.1	Depression rate	13,15
θ_p	3	Calcium threshold for potentiation	15
θ_d	1.2	Calcium threshold for depression	15
σ_{pl}	0.290436 nC s ^{1/2}	Standard deviation for plasticity fluctuations	13,15
α	1	Protein synthesis rate	15,20
θ_{pro}	0.210037 nC	Protein synthesis threshold	15
θ_{tag}	0.0840149 nC	Tagging threshold	15

mechanisms are essential for memory dynamics, and it predicts that these STC mechanisms also allow the improvement of memories, which can be beneficial for biological, as well as artificial memory systems.

Methods

Model. To simulate the dynamics of memory representations, we use a network model with hippocampal characteristics that comprises spiking neurons and synapses with detailed plasticity features. In the following, we first present our mathematical description of neurons and synapses, which is depicted in Fig. 1a. After that, we explain how our network is structured at the population level. The parameters we use are given in Tables 1 and 2.

The dynamics of the membrane potential $V_i(t)$ of the leaky integrate-and-fire neuron i is described by⁹²:

$$\tau_{\text{mem}} \frac{dV_i(t)}{dt} = V_{\text{rev}} - V_i(t) + R \sum_j \sum_{t_j^k} w_{ji}/s \cdot \exp\left(-\frac{(t - t_j^k - t_{\text{ax,delay}})/\tau_{\text{syn}}}{\tau_{\text{syn}}}\right) + R \left(I_{\text{bg}}(t) + I_{\text{stim}}(t) \right) \quad (8)$$

with reversal potential V_{rev} , membrane time constant τ_{mem} , membrane resistance R , synaptic weights w_{ji} , spike times t_j^k , axonal delay time $t_{\text{ax,delay}}$, synaptic time constant τ_{syn} , external background current $I_{\text{bg}}(t)$, and external stimulus current $I_{\text{stim}}(t)$. If V_i crosses the threshold V_{th} , a spike is generated. The spike time t_i^l is then stored and the membrane potential is reset to V_{reset} where it remains for the refractory period t_{ref} . Apart from learning and recall stimulation, the membrane potential dynamics is mainly driven by a background noise current that accounts for synaptic inputs from outside the network, described by an Ornstein–Uhlenbeck process:

$$\tau_{\text{syn}} \frac{dI_{\text{bg}}(t)}{dt} = I_0 - I_{\text{bg}}(t) + \sigma_{\text{wn}} \cdot \Gamma(t) \quad (9)$$

with mean current I_0 and white-noise standard deviation σ_{wn} . Note that in this equation, $\Gamma(t)$ is Gaussian white noise with mean zero and variance $1/dt$ that approaches infinity for $dt \rightarrow 0$ (ref. 93). The Ornstein–Uhlenbeck process has the same colored-noise power spectrum as the fluctuating input to cortical neurons coming from a large presynaptic population⁹⁴. Therefore, it is well-suited to model background noise in our model. In addition to the background noise, a second Ornstein–Uhlenbeck process is used to model the stimulus current $I_{\text{stim}}(t)$ for learning and recall, which is described in the subsection “Learning and recall procedure” below.

If there is a synaptic connection from some neuron j to neuron i , all spikes k that occur in j are transmitted to i . The postsynaptic current caused by a presynaptic spike depends on the weight of the synapse. The total weight or strength of a synaptic connection from neuron j to neuron i is given by:

$$w_{ji} = \begin{cases} h_{ji} + h_0 \cdot z_{ji} & \text{for } E \rightarrow E, \\ w_{ei} & \text{for } E \rightarrow I, \\ w_{ie} & \text{for } I \rightarrow E, \\ w_{ii} & \text{for } I \rightarrow I, \end{cases} \quad (10)$$

where E and I stand for excitatory and inhibitory neurons, respectively. Thus, in our model, all synaptic connections involving inhibitory neurons are constant. The weight of $E \rightarrow E$ connections, however, consists of two variable contributions providing the core of the STC mechanisms: the early-phase weight h_{ji} , and the late-phase weight z_{ji} . We followed¹⁵ and used h_0 as the normalization factor for z to obtain a quantity of the same dimension as h . The value of the normalization factor is in accordance with experiments investigating late-phase LTP/LTD.

The dynamics of the early-phase weight is given by

$$\tau_h \frac{dh_{ji}(t)}{dt} = 0.1 (h_0 - h_{ji}(t)) + \gamma_p (1 \text{ nC} - h_{ji}(t)) \cdot \Theta[c_{ji}(t) - \theta_p] - \gamma_d h_{ji}(t) \cdot \Theta[c_{ji}(t) - \theta_d] + \xi(t), \quad (11)$$

where $\Theta[\cdot]$ is the Heaviside function, τ_h is a time constant, and $c_{ji}(t)$ is the calcium concentration at the postsynaptic site. The first term on the right-hand side describes a relaxation of the early-phase weight back to its initial value h_0 , the second term describes early-phase LTP with rate γ_p for calcium above the threshold θ_p , the third term describes early-phase LTD with rate γ_d for calcium above the threshold θ_d , and the fourth term $\xi(t) = \sqrt{\tau_h[\Theta(c_{ji}(t) - \theta_p) + \Theta(c_{ji}(t) - \theta_d)]} \sigma_{pl} \Gamma(t)$ describes calcium-dependent noise-driven fluctuations with standard deviation σ_{pl} , and Gaussian white noise $\Gamma(t)$ with mean zero and variance $1/dt$. The calcium concentration $c_{ji}(t)$ at the postsynaptic site depends on all past presynaptic and postsynaptic spikes n and m , respectively:

$$\frac{dc_{ji}(t)}{dt} = -\frac{c_{ji}(t)}{\tau_c} + c_{pre} \sum_n \delta(t - t_j^n - t_{c,delay}) + c_{post} \sum_m \delta(t - t_i^m), \quad (12)$$

where $\delta(\cdot)$ is the Dirac delta distribution, τ_c is a time constant, c_{pre} is the contribution of presynaptic spikes, c_{post} is the contribution of postsynaptic spikes, t_j^n and t_i^m are spike times, and $t_{c,delay}$ is the delay of calcium triggered by presynaptic spikes.

The calcium-based plasticity model (Eqs. (11) and (12)) that we use to describe the early phase of LTP and depression is based on previous theoretical studies^{13,15,95}. Similar to Li et al.¹⁵, the first term on the right-hand side of Eq. (11) describes a relaxation to the initial condition to which the early-phase weight returns or decays on a timescale of a few hours. This decay accounts for the fact that early-phase changes are transient, providing an accurate description of the experimentally verified dynamics of the STC mechanisms¹⁸.

The calcium parameters provided by Graupner and Brunel¹³ were obtained by fitting experimental data from in vitro experiments³⁹. Since extracellular calcium concentrations are much lower in vivo than in vitro, the parameters need to be corrected for modeling in vivo networks. Following Higgins et al.⁹⁵, the calcium influx into the postsynaptic spine can be assumed to decrease proportionally to the ratio of in vivo and in vitro extracellular calcium concentrations, which leads to a factor of 0.6. Therefore, in our network model, we adjust the values provided by Graupner and Brunel¹³ by this factor.

Driven by the calcium-based early-phase dynamics, the late-phase synaptic weight is given by

$$\tau_z \frac{dz_{ji}(t)}{dt} = p_i(t) \cdot (1 - z_{ji}(t)) \cdot \Theta[(h_{ji}(t) - h_0) - \theta_{tag}] \quad (13)$$

$$-p_i(t) \cdot (z_{ji} + 0.5) \cdot \Theta[(h_0 - h_{ji}(t)) - \theta_{tag}], \quad (14)$$

with the protein amount $p_i(t)$, the late-phase time constant τ_z , and the tagging threshold θ_{tag} . The first term on the right-hand side describes late-phase LTP, while the second term describes late-phase LTD. Both depend on the amount of proteins being available. If the early-phase weight change $|h_{ji}(t) - h_0|$ exceeds the tagging threshold, the synapse is tagged. This can be the case either for positive or for negative weight changes. The presence of the tag leads to the capture of proteins (if $p_i(t) > 0$), and thereby gives rise to changes in the late-phase weight.

The synthesis of new proteins depends on the early-phase weights, but the amount of proteins also inherently decays exponentially²⁰:

$$\tau_p \frac{dp_i(t)}{dt} = -p_i(t) + \alpha \Theta \left[\left(\sum_j |h_{ji}(t) - h_0| \right) - \theta_{pro} \right]. \quad (15)$$

Using the neuron model and the synapse model explained above, we set up a neural network consisting of 1600 excitatory and 400 inhibitory neurons (depicted in Fig. 1b). This ratio between excitatory and inhibitory neurons is commonly used for cortical and hippocampal networks⁴⁷. Some of the excitatory neurons receive specific inputs to learn and recall a memory representation (see next subsection). As described before, only the synapses between excitatory neurons are plastic. The

inhibitory population serves to provide realistic feedback inhibition. The overall connectivity across both populations is 10%, meaning that there is a probability of 0.1 that the link from any neuron to another one in the whole network exists. The value is reasonable for hippocampal region CA3⁴⁸.

Learning and recall procedure. Before we stimulate our network, we first let the initial activity settle for 10.0 s. After that, we apply our learning protocol, which delivers three stimulus pulses, of 0.1 s duration each, to the neurons belonging to the desired cell assembly (for instance, to the first 150 neurons in the network). The pulses in our protocol are separated by breaks of 0.4 s. During the pulses, stimulation $I_{stim}(t)$ enters the neuronal membrane potential given in Eq. (8). The stimulation is modeled by the following Ornstein-Uhlenbeck process (also cf. Eq. (9)):

$$\tau_{syn} \frac{dI_{stim}(t)}{dt} = w_{stim} \cdot N_{stim} \cdot f_{stim} - I_{stim}(t) + w_{stim} \cdot \sqrt{N_{stim} \cdot f_{stim}} \cdot \Gamma(t), \quad (16)$$

with Gaussian white noise $\Gamma(t)$ and the synaptic time constant τ_{syn} . Mean and standard deviation of the process are defined by putative input spikes from N_{stim} neurons, occurring at the frequency f_{stim} and conveyed by synapses of weight w_{stim} to the selected neurons of our network^{93,96}. For the reproduction of previous single-synapse investigations (ref. 15, Fig. 2), we stimulated the presynaptic neuron with Poisson spikes that were generated using the same number of input neurons N_{stim} and the same frequency f_{stim} as for learning a cell assembly, conveyed with the same synaptic strength w_{stim} .

After 20.0 s, we save the state of the whole network and then apply a recall stimulus, equally modeled by the process given in Eq. (16) with the same parameters as the learning stimulus (except for Supplementary Fig. S7), for 0.1 s to half of the neurons in the cell assembly (regarding the example above, to 75 randomly drawn neurons). We refer to this as “10s-recall”. Next, we load the previously saved network state again, such that the network is back in the state where it was immediately before recall. This time, we let the network run for 28810.0 s until we apply the recall stimulus, which we refer to as “8h-recall”. For one part of our study, we apply a further, intermediate, recall stimulus at a time in between 10 s and 8 h. Following this intermediate recall, we do not reset the network by loading an earlier state, such that it in fact affects the later 8h-recall.

Measures of recall performance. To investigate the effects of recall stimulation, we divide the excitatory population into three subpopulations: control neurons that are not directly stimulated neither by learning nor by recall stimulation, cell assembly neurons that are stimulated by both learning and recall stimulus, and cell assembly neurons that are stimulated during learning but not during recall (cf. Fig. 3d). The mean activities of these three subpopulations are given by:

- \bar{v}_{as} : mean activity of the neurons stimulated by the learning stimulus and the recall stimulus
as = “assembly, stimulated”
- \bar{v}_{ans} : mean activity of the neurons stimulated by the learning stimulus but not by the recall stimulus
ans = “assembly, not stimulated”
- \bar{v}_{ctrl} : mean activity of the neurons stimulated by neither of the two stimuli
ctrl = “control”

Based on these mean activities, the recall quality can be measured by computing a coefficient for the quality of pattern completion:

$$Q^* := \frac{\bar{v}_{ans} - \bar{v}_{ctrl}}{\bar{v}_{as}}. \quad (17)$$

The coefficient typically lies within the interval (0, 1). To achieve pattern completion of the learning-defined cell assembly, the non-stimulated assembly neurons have to be indirectly activated following the activation of the rest of the core neurons, while control neurons should remain relatively silent:

$$\bar{v}_{ctrl} \ll \bar{v}_{ans} \leq \bar{v}_{as}. \quad (18)$$

Hence, for good pattern completion or good recall, the value of Q^* will be significantly larger than zero or even approach unity. On the other hand, if it approaches zero, there is either no pattern completion, which means that $\bar{v}_{ctrl} \approx \bar{v}_{ans}$, or the network activity diverges, which means that $\bar{v}_{ctrl} \approx \bar{v}_{ans} \approx \bar{v}_{as}$.

In addition to the subpopulation-based quantity Q^* , we measure the mutual information MI_v between the activity distribution during the recall phase and the activity distribution during the learning phase. The mutual information does not directly relate to pattern completion, but it has the advantage that it is independent of any predefined patterns such as the learning stimulus.

The mutual information of the activity distribution is calculated from the entropy during the learning phase at time $t_{learn} = 11.0$ s, the entropy during the

recall phase at time $t_{\text{recall}} \in \{20.1 \text{ s}, 28810.1 \text{ s}\}$, and the joint entropy between both:

$$MI_{\nu} := H(\nu(t = t_{\text{learn}}, n)) + H(\nu(t = t_{\text{recall}}, n)) - H(\nu(t = t_{\text{learn}}, n), \nu(t = t_{\text{recall}}, n)). \quad (19)$$

The firing rate function $\nu(t, n)$ returns the firing rate of a given neuron n at a given time t , computed using a sliding window of 0.5 s.

Statistics and reproducibility. The pattern completion effect is not necessarily robust across trials for every parameter setting, even though $Q^* \gg 0$ may be given for a single trial. Therefore, we average over trials:

$$Q := \langle Q^* \rangle. \quad (20)$$

For Fig. 4, due to the lack of error bars, we have to indicate the cases in which no robust pattern completion occurs. Thus, we use the following conditional definition for the pattern completion coefficient:

$$Q := \begin{cases} \langle Q^* \rangle & \text{if } \langle Q^* \rangle > \Delta Q, \\ 0 & \text{else.} \end{cases} \quad (21)$$

Put in words, the robustness criterion requires the mean $\langle Q^* \rangle$ to be nonnegative, and its absolute value to be larger than the standard deviation ΔQ . If this is not fulfilled, pattern completion is assumed absent and Q is set to zero.

To achieve equal statistics for our results, we also average the mutual information value over multiple trials and use the standard deviation as error.

The relative gain in recall quality after 8 h as compared to recall quality after 10 s is computed by $\frac{Q(8 \text{ h}) - Q(10 \text{ s})}{Q(10 \text{ s})}$ for the coefficient Q , and $\frac{(MI_{\nu}(8 \text{ h}) - (MI_{\nu}(10 \text{ s})))}{(MI_{\nu}(10 \text{ s}))}$ for the mutual information. The error of the relative gain is computed by propagation of error from the recall quality at 10 s and at 8 h, such that it is

$$\sqrt{\left(\frac{\Delta Q(10 \text{ s}) - Q(8 \text{ h})}{Q(10 \text{ s})}\right)^2 + \left(\frac{\Delta Q(8 \text{ h})}{Q(10 \text{ s})}\right)^2} \text{ for } Q \text{ and } \sqrt{\left(\frac{\Delta MI_{\nu}(10 \text{ s}) \cdot (MI_{\nu}(8 \text{ h}))}{(MI_{\nu}(10 \text{ s}))^2}\right)^2 + \left(\frac{\Delta MI_{\nu}(8 \text{ h})}{(MI_{\nu}(10 \text{ s}))}\right)^2}$$

for the mutual information. Our approach to determine significant effects is to compute and compare standard deviations of observables from at least ten trials. The number of simulation trials (100 for single-synapse simulations, 10 for learning and recall simulations) was chosen such that the effects that we describe would be significant with $p < 0.006$ in a t test. This is the case for a single observable being greater than zero, if zero is not within the standard deviation of the observable (one-sided test), and also for the inequality of two observables if their standard deviations do not overlap (two-sided test, cf.⁹⁷), because for the chosen number of trials the standard deviation is greater than the 98.8% confidence interval.

The network structure that we used to obtain the results presented here is provided with our code⁹⁸. The code automatically generates a different network structure with the same connectivity p_c if no predefined structure is used. We did not encounter unexpected deviations with such different network structures.

Computational implementation and software used. We used C++ in the ISO 2011 standard to implement our simulations. To compile and link the code, we employed g++ in version 7.4.0 with boost in version 1.65.1.

Random numbers were generated using the generator `minstd_rand0` from the C++ standard library, while the system time served as the seed. We implemented a loop in our code which ensured that for each distribution a unique seed was used.

For the creation of plots, we used gnuplot 5.0.3, as well as Matplotlib 2.0.0 with Python 3.6.8 and NumPy 1.16.4.

The network simulations that we needed to perform for this study were computationally extremely demanding. Fortunately, we had the opportunity to use the computing cluster of the Gesellschaft für wissenschaftliche Datenverarbeitung mbH Göttingen (GWDG), which enables fast computation on a large set of processing units. However, despite this strong computational power and the usage of compiled C++ code, running our spiking network simulations in full detail still took unacceptably long. Thus, to be able to simulate our network faster, we used an approximation that neglects the spiking dynamics in periods without external stimulation. In these periods, we just computed the late-phase dynamics and the exponential decay of the early-phase weights. Supplementary Fig. S2 shows that this approach is justified because the weight dynamics of a synapse does not change if sparsely occurring spikes are neglected. Furthermore, the mutual information conveyed by 8h-recall is in the same regime for full and approximating computation.

Reporting summary. Further information on research design is available in the Nature Research Reporting Summary linked to this article.

Data availability

The data underlying the results presented in this study can be reproduced using the simulation code and the analysis scripts that we have released⁹⁸. Furthermore, we provide the Source data for the Figures in this article in Supplementary Data 1 and 2.

Code availability

Our simulation code, along with scripts to analyze the data, has been released at <https://doi.org/10.5281/zenodo.4429196> and can be retrieved freely⁹⁸.

Received: 29 May 2020; Accepted: 21 January 2021;

Published online: 03 March 2021

References

- Dudai, Y. The neurobiology of consolidation, or, how stable is the engram? *Annu. Rev. Psychol.* **55**, 51–86 (2004).
- Gluck, M. A., Mercado, E. & Myers, C. E. *Learning and Memory: From Brain to Behavior* 3rd edn (Worth Publishers, 2016).
- Eichenbaum, H. *The Cognitive Neuroscience of Memory: an Introduction* 2nd edn (Oxford University Press, 2011).
- Eichenbaum, H. Barlow versus Hebb: When is it time to abandon the notion of feature detectors and adopt the cell assembly as the unit of cognition? *Neurosci. Lett.* **680**, 88–93 (2017).
- Hebb, D. O. *The Organization of Behavior* 1st edn (Wiley, 1949).
- Martin, S. J., Grimwood, P. D. & Morris, R. G. Synaptic plasticity and memory: an evaluation of the hypothesis. *Ann. Rev. Neurosci.* **23**, 649–711 (2000).
- Artola, A. & Singer, W. Long-term depression of excitatory synaptic transmission and its relationship to long-term potentiation. *Trends Neurosci.* **16**, 480–487 (1993).
- Bear, M. F. A synaptic basis for memory storage in the cerebral cortex. *Proc. Natl. Acad. Sci. USA* **93**, 13453–13459 (1996).
- Abraham, W. C., Jones, O. D. & Glanzman, D. L. Is plasticity of synapses the mechanism of long-term memory storage? *NPJ Sci. Learn.* **4**, 1–10 (2019).
- Artola, A., Bröcher, S. & Singer, W. Different voltage-dependent thresholds for inducing long-term depression and long-term potentiation in slices of rat visual cortex. *Nature* **347**, 69–72 (1990).
- Bliss, T. V. & Collingridge, G. L. A synaptic model of memory: long-term potentiation in the hippocampus. *Nature* **361**, 31 (1993).
- Smolen, P., Baxter, D. A. & Byrne, J. H. Molecular constraints on synaptic tagging and maintenance of long-term potentiation: a predictive model. *PLoS Comput. Biol.* **8**, e1002620 (2012).
- Graupner, M. & Brunel, N. Calcium-based plasticity model explains sensitivity of synaptic changes to spike pattern, rate, and dendritic location. *Proc. Natl. Acad. Sci. USA* **109**, 3991–3996 (2012).
- Hansel, C., Artola, A. & Singer, W. Different threshold levels of postsynaptic $[Ca^{2+}]_i$ have to be reached to induce LTP and LTD in neocortical pyramidal cells. *J. Physiol. Paris* **90**, 317–319 (1996).
- Li, Y., Kulvicius, T. & Tetzlaff, C. Induction and consolidation of calcium-based homo- and heterosynaptic potentiation and depression. *PLoS ONE* **11**, e0161679 (2016).
- Shouval, H., Bear, M. & Cooper, L. A unified model of NMDA receptor-dependent bidirectional synaptic plasticity. *Proc. Natl. Acad. Sci. USA* **99**, 10831–10836 (2002).
- Abraham, W. C. How long will long term potentiation last? *Phil. Trans. R. Soc. Lond. B* **358**, 735–744 (2003).
- Frey, U. & Morris, R. G. M. Synaptic tagging and long-term potentiation. *Nature* **385**, 533–536 (1997).
- Redondo, R. L. & Morris, R. G. M. Making memories last: the synaptic tagging and capture hypothesis. *Nat. Rev. Neurosci.* **12**, 17–30 (2011).
- Clopath, C., Ziegler, L., Vasilaki, E., Büsing, L. & Gerstner, W. Tag-trigger-consolidation: a model of early and late long-term potentiation and depression. *PLoS Comput. Biol.* **4**, e10000248 (2008).
- Müller, G. & Pilzecker, A. *Experimentelle Beiträge zur Lehre vom Gedächtnis* (Verlag von J. A. Barth, 1900).
- Okuda, K., Højgaard, K., Privitera, L., Bayraktar, G. & Takeuchi, T. Initial memory consolidation and the synaptic tagging and capture hypothesis. *Eur. J. Neurosci.* **00**, 1–24 (2020).
- Nadel, L. & Moscovitch, M. Memory consolidation, retrograde amnesia and the hippocampal complex. *Curr. Opin. Neurobiol.* **7**, 217–227 (1997).
- McGaugh, J. Memory - a century of consolidation. *Science* **287**, 248–251 (2000).
- Clopath, C. Synaptic consolidation: an approach to long-term learning. *Cogn. Neurodyn.* **6**, 251–257 (2012).
- Dudai, Y., Karni, A. & Born, J. The consolidation and transformation of memory. *Neuron* **88**, 20–32 (2015).
- Barrett, A. B., Billings, G. O., Morris, R. G. M. & van Rossum, M. C. W. State based model of long-term potentiation and synaptic tagging and capture. *PLoS Comput. Biol.* **5**, e1000259 (2009).
- Ziegler, L., Zenke, F., Kastner, D. B. & Gerstner, W. Synaptic consolidation: from synapses to behavioral modeling. *J. Neurosci.* **35**, 1319–1334 (2015).
- Zenke, F., Agnes, E. J. & Gerstner, W. Diverse synaptic plasticity mechanisms orchestrated to form and retrieve memories in spiking neural networks. *Nat. Commun.* **6**, 1–13 (2015).
- Bi, G.-q. & Poo, M.-m. Synaptic modifications in cultured hippocampal neurons: dependence on spike timing, synaptic strength, and postsynaptic cell type. *J. Neurosci.* **18**, 10464–10472 (1998).

31. Letzkus, J. J., Kampa, B. M. & Stuart, G. J. Learning rules for spike timing-dependent plasticity depend on dendritic synapse location. *J. Neurosci.* **26**, 10420–10429 (2006).
32. Nevian, T. & Sakmann, B. Spine Ca²⁺ signaling in spike-timing-dependent plasticity. *J. Neurosci.* **26**, 11001–11013 (2006).
33. O'Connor, D. H., Wittenberg, G. M. & Wang, S. S.-H. Dissection of bidirectional synaptic plasticity into saturable unidirectional processes. *J. Neurophysiol.* **94**, 1565–1573 (2005).
34. Reymann, K. G. & Frey, J. U. The late maintenance of hippocampal LTP: requirements, phases, 'synaptic tagging', 'late-associativity' and implications. *Neuropharmacology* **52**, 24–40 (2007).
35. Sajikumar, S., Navakkode, S. & Frey, J. U. Identification of compartment- and process-specific molecules required for "synaptic tagging" during long-term potentiation and long-term depression in hippocampal CA1. *J. Neurosci.* **27**, 5068–5080 (2007).
36. Sjöström, P. J., Turrigiano, G. G. & Nelson, S. B. Rate, timing, and cooperativity jointly determine cortical synaptic plasticity. *Neuron* **32**, 1149–1164 (2001).
37. Sjöström, P. J. & Häusser, M. A cooperative switch determines the sign of synaptic plasticity in distal dendrites of neocortical pyramidal neurons. *Neuron* **51**, 227–238 (2006).
38. Wang, H.-X., Gerkin, R. C., Nauen, D. W. & Bi, G.-Q. Coactivation and timing-dependent integration of synaptic potentiation and depression. *Nat. Neurosci.* **8**, 187–193 (2005).
39. Wittenberg, G. M. & Wang, S. S.-H. Malleability of spike-timing-dependent plasticity at the CA3–CA1 synapse. *J. Neurosci.* **26**, 6610–6617 (2006).
40. Elliott, T. & Lagogiannis, K. The rise and fall of memory in a model of synaptic integration. *Neural Comput.* **24**, 2604–2654 (2012).
41. Fusi, S., Drew, P. J. & Abbott, L. F. Cascade models of synaptically stored memories. *Neuron* **45**, 599–611 (2005).
42. Elliott, T. The enhanced rise and delayed fall of memory in a model of synaptic integration: extension to discrete state synapses. *Neural Comput.* **28**, 1927–1984 (2016).
43. Benna, M. K. & Fusi, S. Computational principles of synaptic memory consolidation. *Nat. Neurosci.* **19**, 1697–1706 (2016).
44. Papper, M., Kempster, R. & Leibold, C. Synaptic tagging, evaluation of memories, and the distal reward problem. *Learn. Mem.* **18**, 58–70 (2011).
45. Gerstner, W. & Naud, R. How good are neuron models? *Science* **326**, 379–380 (2009).
46. Tchumatchenko, T., Malyshev, A., Wolf, F. & Volgushev, M. Ultrafast population encoding by cortical neurons. *J. Neurosci.* **31**, 12171–12179 (2011).
47. Braitenberg, V. & Schüz, A. *Cortex: Statistics and Geometry of Neuronal Connectivity* 2nd edn (Springer, 1998).
48. Le Duigou, C., Simonnet, J., Teleńczuk, M., Fricker, D. & Miles, R. M. Recurrent synapses and circuits in the CA3 region of the hippocampus: an associative network. *Front. Cell. Neurosci.* **7**, 262 (2014).
49. Mizuseki, K. & Buzsáki, G. Preconfigured, skewed distribution of firing rates in the hippocampus and entorhinal cortex. *Cell Rep.* **4**, 1010–1021 (2013).
50. Mizuseki, K. & Miyawaki, H. Hippocampal information processing across sleep/wake cycles. *Neurosci. Res.* **118**, 30–47 (2017).
51. Sajikumar, S., Navakkode, S., Sacktor, T. C. & Frey, J. U. Synaptic tagging and cross-tagging: the role of protein kinase M ζ in maintaining long-term potentiation but not long-term depression. *J. Neurosci.* **25**, 5750–5756 (2005).
52. Sajikumar, S. & Frey, J. U. Resetting of 'synaptic tags' is time- and activity-dependent in rat hippocampal *in vitro*. *Neuroscience* **129**, 503–507 (2004).
53. Tetzlaff, C., Dasgupta, S., Kulvicius, T. & Wörgötter, F. The use of hebbian cell assemblies for nonlinear computation. *Sci. Rep.* **5**, 12866 (2015).
54. Denève, S. & Machens, C. K. Efficient codes and balanced networks. *Nat. Neurosci.* **19**, 375 (2016).
55. Erdelyi, M. H. & Kleinbard, J. Has Ebbinghaus decayed with time? The growth of recall (hypermnnesia) over days. *J. Exp. Psychol. Hum. Learn.* **4**, 275 (1978).
56. Payne, D. G. Hypermnnesia and reminiscence in recall: a historical and empirical review. *Psychol. Bull.* **101**, 5 (1987).
57. Wallner, L. A. & Bäuml, K.-H. T. Hypermnnesia and the role of delay between study and test. *Mem. Cogn.* **46**, 878–894 (2018).
58. Graupner, M. & Brunel, N. Mechanisms of induction and maintenance of spike-timing dependent plasticity in biophysical synapse models. *Front. Comput. Neurosci.* **4**, 136 (2010).
59. Ranganath, C., Cohen, M. X. & Brozinsky, C. J. Working memory maintenance contributes to long-term memory formation: neural and behavioral evidence. *J. Cogn. Neurosci.* **17**, 994–1010 (2005).
60. O'Reilly, R., Braver, T. & Cohen, J. in *Models of Working Memory: Mechanisms of Active Maintenance and Executive Control*, Chap. 11 (Cambridge University Press, 1999).
61. Nachstedt, T. & Tetzlaff, C. Working memory requires a combination of transient and attractor-dominated dynamics to process unreliably timed inputs. *Sci. Rep.* **7**, 1–14 (2017).
62. Vogels, T. P., Sprekeler, H., Zenke, F., Clopath, C. & Gerstner, W. Inhibitory plasticity balances excitation and inhibition in sensory pathways and memory networks. *Science* **334**, 1569–1573 (2011).
63. Sprekeler, H. Functional consequences of inhibitory plasticity: homeostasis, the excitation-inhibition balance and beyond. *Curr. Opin. Neurobiol.* **43**, 198–203 (2017).
64. Racine, R., Milgram, N. & Hafner, S. Long-term potentiation phenomena in the rat limbic forebrain. *Brain Res.* **260**, 217–231 (1983).
65. Abraham, W. C., Logan, B., Greenwood, J. M. & Dragunow, M. Induction and experience-dependent consolidation of stable long-term potentiation lasting months in the hippocampus. *J. Neurosci.* **22**, 9626–9634 (2002).
66. Landry, C. D., Kandel, E. R. & Rajasethupathy, P. New mechanisms in memory storage: piRNAs and epigenetics. *Trends Neurosci.* **36**, 535–542 (2013).
67. Scoville, W. & Milner, B. Loss of recent memory after bilateral hippocampal lesions. *J. Neurol. Neurosurg. Psychiatry* **20**, 11–21 (1957).
68. Rasch, B. & Born, J. About sleep's role in memory. *Physiol. Rev.* **93**, 681–766 (2013).
69. Tetzlaff, C., Kolodziejcki, C., Timme, M., Tsodyks, M. & Wörgötter, F. Synaptic scaling enables dynamically distinct short- and long-term memory formation. *PLoS Comput. Biol.* **9**, e1003307 (2013).
70. Seidenbecher, T., Reymann, K. G. & Balschun, D. A post-tetanic time window for the reinforcement of long-term potentiation by appetitive and aversive stimuli. *Proc. Natl. Acad. Sci. USA* **94**, 1494–1499 (1997).
71. Jahnke, S., Timme, M. & Memmesheimer, R.-M. A unified dynamic model for learning, replay, and sharp-wave/ripples. *J. Neurosci.* **35**, 16236–16258 (2015).
72. Martin, K. C. et al. Synapse-specific, long-term facilitation of aplysia sensory to motor synapses: a function for local protein synthesis in memory storage. *Cell* **91**, 927–938 (1997).
73. Jiang, C. & Schuman, E. M. Regulation and function of local protein synthesis in neuronal dendrites. *Trends Biochem. Sci.* **27**, 506–513 (2002).
74. Bramham, C. R. Local protein synthesis, actin dynamics, and LTP consolidation. *Curr. Opin. Neurobiol.* **18**, 524–531 (2008).
75. O'Donnell, C. & Sejnowski, T. J. Selective memory generalization by spatial patterning of protein synthesis. *Neuron* **82**, 398–412 (2014).
76. Kastellakis, G. I. & Poirazi, P. Synaptic clustering and memory formation. *Front. Mol. Neurosci.* **12**, 300 (2019).
77. Erdelyi, M. H. The ups and downs of memory. *Am. Psychol.* **65**, 623 (2010).
78. Bjork, R. A. & Bjork, E. L. In *From learning processes to cognitive processes: Essays in honor of William K. Estes*, Vol. 2, Ch. 2 (L. Erlbaum, 1992).
79. Karpicke, J. D., Lehman, M. & Aue, W. R. Retrieval-based learning: an episodic context account. *Psychol. Learn. Motiv.* **61**, 237–284 (2014).
80. Moncada, D. & Viola, H. Induction of long-term memory by exposure to novelty requires protein synthesis: evidence for a behavioral tagging. *J. Neurosci.* **27**, 7476–7481 (2007).
81. Ballarini, F., Moncada, D., Martinez, M. C., Alen, N. & Viola, H. Behavioral tagging is a general mechanism of long-term memory formation. *Proc. Natl. Acad. Sci. USA* **106**, 14599–14604 (2009).
82. Moncada, D., Ballarini, F. & Viola, H. Behavioral tagging: a translation of the synaptic tagging and capture hypothesis. *Neural Plast.* **2015**, 650780 (2015).
83. Liu, M.-G., Chen, X.-F., He, T., Li, Z. & Chen, J. Use of multi-electrode array recordings in studies of network synaptic plasticity in both time and space. *Neurosci. Bull.* **28**, 409–422 (2012).
84. Akerboom, J. et al. Genetically encoded calcium indicators for multi-color neural activity imaging and combination with optogenetics. *Front. Mol. Neurosci.* **6**, 2 (2013).
85. Stamatakis, A. M. et al. Simultaneous optogenetics and cellular resolution calcium imaging during active behavior using a miniaturized microscope. *Front. Neurosci.* **12**, 496 (2018).
86. Chetthi, S. N. & Harvey, C. D. Single-neuron perturbations reveal feature-specific competition in V1. *Nature* **567**, 334–340 (2019).
87. Russell, L. E. et al. The influence of visual cortex on perception is modulated by behavioural state. Preprint at *bioRxiv* <https://doi.org/10.1101/706010> (2019).
88. Luboinski, J. & Tchumatchenko, T. Nonlinear response characteristics of neural networks and single neurons undergoing optogenetic excitation. *Netw. Neurosci.* **4**, 852–870 (2020).
89. Davies, M. et al. Loihi: a neuromorphic manycore processor with on-chip learning. *IEEE Micro* **38**, 82–99 (2018).
90. Lin, C.-K. et al. Programming spiking neural networks on intel's Loihi. *Computer* **51**, 52–61 (2018).
91. Wang, Q., Li, Y., Shao, B., Dey, S. & Li, P. Energy efficient parallel neuromorphic architectures with approximate arithmetic on FPGA. *Neurocomputing* **221**, 146–158 (2017).
92. Gerstner, W. & Kistler, W. M. *Spiking Neuron Models* 1st edn (Cambridge University Press, 2002).
93. Gillespie, D. T. Exact numerical simulation of the ornstein-uhlenbeck process and its integral. *Phys. Rev. E* **54**, 2084–2091 (1996).

94. Destexhe, A., Rudolph, M. & Paré, D. The high-conductance state of neocortical neurons in vivo. *Nat. Rev. Neurosci.* **4**, 739–751 (2003).
95. Higgins, D., Graupner, M. & Brunel, N. Memory maintenance in synapses with calcium-based plasticity in the presence of background activity. *PLoS Comput. Biol.* **10**, e1003834 (2014).
96. Dayan, P. & Abbott, L. F. *Theoretical Neuroscience* 1st edn (The MIT Press, 2001).
97. Payton, M. E., Greenstone, M. H. & Schenker, N. Overlapping confidence intervals or standard error intervals: what do they mean in terms of statistical significance? *J. Insect Sci.* **3**, 34 (2003).
98. Luboinski, J. Simulation code and analysis scripts. <https://doi.org/10.5281/zenodo.4429196> (2021).
99. Roth, A. & van Rossum, M. C. W. *Computational Modeling Methods for Neuroscientists* 1st edn (The MIT Press, 2009).
100. Lin, J.-W. & Faber, D. S. Modulation of synaptic delay during synaptic plasticity. *Trends Neurosci.* **25**, 449–455 (2002).
101. Kobayashi, R., Tsubo, Y. & Shinomoto, S. Made-to-order spiking neuron model equipped with a multi-timescale adaptive threshold. *Front. Comput. Neurosci.* **3**, 9 (2009).

Acknowledgements

We would like to thank the members of the Department of Computational Neuroscience for many fruitful discussions and various helpful comments on this study. The research was funded by the German Research Foundation (CRC1286, project C1, project #419866478) and by the H2020-FETPROACT project Plan4Act (#732266).

Author contributions

J.L.: conceptualization; data curation; formal analysis; investigation; methodology; software; validation; visualization; and writing and editing. C.T.: conceptualization; funding acquisition; investigation; methodology; project administration; resources; supervision; and writing and editing.

Funding

Open Access funding enabled and organized by Projekt DEAL.

Competing interests

The authors declare no competing interests.

Additional information

Supplementary information The online version contains supplementary material available at <https://doi.org/10.1038/s42003-021-01778-y>.

Correspondence and requests for materials should be addressed to J.L. or C.T.

Reprints and permission information is available at <http://www.nature.com/reprints>

Publisher's note Springer Nature remains neutral with regard to jurisdictional claims in published maps and institutional affiliations.



Open Access This article is licensed under a Creative Commons Attribution 4.0 International License, which permits use, sharing, adaptation, distribution and reproduction in any medium or format, as long as you give appropriate credit to the original author(s) and the source, provide a link to the Creative Commons license, and indicate if changes were made. The images or other third party material in this article are included in the article's Creative Commons license, unless indicated otherwise in a credit line to the material. If material is not included in the article's Creative Commons license and your intended use is not permitted by statutory regulation or exceeds the permitted use, you will need to obtain permission directly from the copyright holder. To view a copy of this license, visit <http://creativecommons.org/licenses/by/4.0/>.

© The Author(s) 2021